

1-1-2006

## On evaluating density driven groundwater flow in the closed basin

Aron M Habte

*University of Nevada, Las Vegas*

Follow this and additional works at: <https://digitalscholarship.unlv.edu/rtds>

---

### Repository Citation

Habte, Aron M, "On evaluating density driven groundwater flow in the closed basin" (2006). *UNLV Retrospective Theses & Dissertations*. 1940.

<http://dx.doi.org/10.25669/rjux-ybo3>

This Thesis is protected by copyright and/or related rights. It has been brought to you by Digital Scholarship@UNLV with permission from the rights-holder(s). You are free to use this Thesis in any way that is permitted by the copyright and related rights legislation that applies to your use. For other uses you need to obtain permission from the rights-holder(s) directly, unless additional rights are indicated by a Creative Commons license in the record and/or on the work itself.

This Thesis has been accepted for inclusion in UNLV Retrospective Theses & Dissertations by an authorized administrator of Digital Scholarship@UNLV. For more information, please contact [digitalscholarship@unlv.edu](mailto:digitalscholarship@unlv.edu).

ON EVALUATING DENSITY DRIVEN GROUNDWATER FLOW IN THE CLOSED  
BASIN

by

Aron M. Habte

Bachelor of Science  
University of Asmara, Eritrea  
1996

A thesis submitted in partial fulfillment  
of the requirements for the

**Master of Science Degree in Water Resource Management  
Department of Water Resource Management  
College of Sciences**

**Graduate College  
University of Nevada, Las Vegas  
May 2006**

UMI Number: 1436753

### INFORMATION TO USERS

The quality of this reproduction is dependent upon the quality of the copy submitted. Broken or indistinct print, colored or poor quality illustrations and photographs, print bleed-through, substandard margins, and improper alignment can adversely affect reproduction.

In the unlikely event that the author did not send a complete manuscript and there are missing pages, these will be noted. Also, if unauthorized copyright material had to be removed, a note will indicate the deletion.

**UMI<sup>®</sup>**

---

UMI Microform 1436753

Copyright 2006 by ProQuest Information and Learning Company.

All rights reserved. This microform edition is protected against unauthorized copying under Title 17, United States Code.

ProQuest Information and Learning Company  
300 North Zeeb Road  
P.O. Box 1346  
Ann Arbor, MI 48106-1346



## Thesis Approval

The Graduate College  
University of Nevada, Las Vegas

April 12, 20 06

The Thesis prepared by

Aron M. Habte

Entitled

On Evaluating Density Driven Groundwater Flow in the Closed Basin

is approved in partial fulfillment of the requirements for the degree of

Master of Science in Water Resource Management

Zhongbo Yu

Examination Committee Chair

Al. Shere

Dean of the Graduate College

[Signature]

Examination Committee Member

David R. Meane

Examination Committee Member

Sharon C. Smith

Graduate College Faculty Representative

## ABSTRACT

### **On Evaluating Density Driven Groundwater Flow in the Closed Basin**

by

Aron M. Habte

Dr. Zhongbo Yu, Examination Committee Chair  
Associate Professor of Hydrogeology  
University of Nevada, Las Vegas

The hydrogeochemical cycle in the Pilot Valley, a closed basin, is subject to climate variability over a wide range of spatial and temporal scales over long period of time. Saturated and Unsaturated Transport Model (SUTRA) is employed in the Pilot Valley to simulate subsurface and density driven groundwater flow under various climatic and geologic conditions. A Maxey-Eakin method with coupled catchment model, aridity index and incomplete beta function for groundwater recharge distribution is integrated into the SUTRA model for various simulations. A Rayleigh number is used to analyze these circulation patterns of flow under variable climate and geologic conditions. The simulation results, under different groundwater recharge rates, indicate the existence or absence of free convection flow and salt nose movement under the playa and towards hinge line. The simulation result for a historical wet period (12 ka) has a narrow salt nose extent and a historical dry period (6 ka) has a wider salt nose extent. High permeability

values generate more free convective cells and low permeability values generate less or eliminate free convective cells in the flow domain. This study will help minimize damage from extreme climatic conditions which occur frequently in the study area and also help manage water resources efficiently.

## TABLE OF CONTENTS

ABSTRACT.....	iii
LIST OF FIGURES .....	viii
ACKNOWLEDGMENTS .....	ix
CHAPTER 1 INTRODUCTION .....	1
1.1 Introduction and Literature Review .....	1
1.2 Description of Study Area .....	3
1.2.1 Location .....	3
1.2.2 Geology.....	5
1.2.3 Climate and Hydrology.....	8
1.3 Scope and Objectives.....	10
CHAPTER 2 METHODOLOGY AND MODEL SIMULATIONS .....	12
2.1 Methods Associated with Factors Affecting Groundwater Flow in a Closed Basin	12
2.1.1 Climatic Variability .....	12
2.1.2 Geologic Heterogeneity .....	14
2.1.3 Scaling Issue .....	15
2.1.4 Groundwater Recharge Estimation and Saline Concentration Distribution .....	17
2.1.4.1 Groundwater Recharge Estimation Using Maxey-Eakin Method .....	18
2.1.4.2 Saline Distribution .....	22
2.2 Saturated and Unsaturated Transport Model (SUTRA).....	24
2.2.1 Model Processes.....	26
2.2.2 Model Application and Example .....	26
2.2.3 Model Parameters for Study Area.....	29
2.2.4 Numerical Method for the Simulation of Fluid and Solute Transport.....	32
2.2.5 Physical Parameters .....	35
CHAPTER 3 DISCUSSIONS AND RESULTS .....	37
3.1 Climatic Variability, Groundwater Flow and Solute Transport.....	37
3.2 Simulations of Advective and Convective Flows under Homogeneous Condition .....	40
3.2.1 Simulation Results for Differing Time Series .....	41
3.2.1.1 Initial Condition .....	42
3.2.1.2 Modern Condition.....	43

3.2.1.3 Simulation Result for 6 ka .....	44
3.2.1.4 Simulation Result for 9 ka .....	45
3.2.1.5 Simulation Result for 12 ka .....	46
3.2.1.6 Simulation Result for 15 ka .....	47
3.2.1.7 Simulation Result for 18 ka .....	48
3.3 Geologic Variability.....	51
3.3.1 Geologic Variability under Wet Period .....	51
3.3.2 Geologic Variability under Dry Period.....	54
CHAPTER 4 CONCLUSIONS AND RECOMMENDATIONS.....	58
APPENDIX 1 RECHARGE DISTRIBUTION FOR FOR ALL PERIODS.....	62
REFERENCES .....	80
VITA.....	86



## LIST OF FIGURES

Figure 1.1	Extent of pluvial lakes, playa basins and existing salt lakes of the Great Basin (from Fan et al., 1997). .....	4
Figure 1.2	Geology of Pilot Valley and the Bonneville Salt Flats of the Great Salt Lake Desert (from Lines, 1979). .....	6
Figure 1.3	Stratigraphic relationships between four major geologic units of the Great Basin (from Lines, 1979). .....	7
Figure 1.4	Conceptual model showing types of groundwater flow in a closed desert basin. $\sigma$ and $L-\sigma$ show the length of recharge and discharge areas respectively (from Duffy and Al-Hassen, 1988). .....	10
Figure 2.1	Heterogeneity of the basin-scale aquifer resulting in different permeability values (after Fan et al., 1997). .....	15
Figure 2.2	Elevation profiles versus distance from the playa to the mountain divide for the study area (data taken from U.S. Geological Survey topographic contour maps) (Duffy and Al-Hassan, 1988). .....	16
Figure 2.3	Normalized scaling relationship of elevation-distance from the incomplete beta function program. ....	17
Figure 2.4	Modern precipitation distributions versus elevation based on Maxey-Eakin method (data from Appendix 1). .....	20
Figure 2.5	Elevation distributions and approximated profile location of the study area - Pilot Valley .....	21
Figure 2.6	Parabolic distribution of saline concentration through time along the specified concentration nodes, based on the notion of the reconstructed Lake Bonneville stage at the end of pleistocene. ....	24
Figure 2.7	Finite element mesh and boundary condition for Henry 1964 solution (Voss et al., 2002). ....	28
Figure 2.8	Simulated velocity fields and salt concentrations for Henry 1964 (Legend shows salt concentration in $\text{kg kg}^{-1}$ units). ....	29
Figure 2.9	Mathematical representation of the conceptual model with its boundary, geometry and initial conditions (from Duffy and Al-Hassan, 1988). ....	30
Figure 2.10	Finite-element grid used in half-basin simulation ( $41 \times 11$ arrays of nodes) and cell, element and nodewise discretization for a two dimensional finite element mesh. ....	31
Figure 3.1	Precipitation distributions versus elevation for the past 20 ka based on Maxey-Eakin method and coupled catchment-lake model (Appendix 1).. ...	38
Figure 3.2	Distribution of precipitation, temperature and groundwater recharge using the Maxey-Eakin method with coupled catchment-lake model and aridity index. ....	39

Figure 3.3	Steady state distributions (a) velocity fields and (b) playa concentrations under initial condition (legend shows kilogram of solute per kilogram of water ( $\text{kg}\text{kg}^{-1}$ )).	43
Figure 3.4	Steady state distributions (a) velocity fields and (b) playa concentrations and salt-extent under modern condition.	44
Figure 3.5	Steady state distributions (a) velocity fields and (b) playa concentrations and salt-nose extent for 6 ka.	45
Figure 3.6	Steady state distributions (a) velocity fields and (b) playa concentrations and salt-nose extent for 9 ka.	46
Figure 3.7	Steady state distributions (a) velocity fields and (b) playa concentrations and salt-nose extent for 12 ka.	47
Figure 3.8	Steady state distributions (a) velocity fields and (b) playa concentrations and salt-nose extent for 15 ka.	48
Figure 3.9	Steady state distributions (a) velocity fields and (b) playa concentrations and salt-nose extent for 18 ka.	49
Figure 3.10	Extent of mixing zone or interface between fresh and saline water.	50
Figure 3.11	Effect of geologic variability (high permeability) and formation of free convective flow: (a) velocity fields and (b) playa concentrations and salt-nose extent for the wet period (12 ka).	52
Figure 3.12	Effect of geologic variability (low permeability) and formation of free convective flow: (a) velocity fields and (b) playa concentrations and salt-nose extent for the wet period (12 ka).	53
Figure 3.13	Effect of geologic variability (high permeability) and formation of free convective flow: (a) velocity fields and (b) playa concentrations and salt-nose extent for the dry period (6 ka).	55
Figure 3.14	Effect of geologic variability (low permeability) and formation of free convective flow (a) velocity fields and (b) playa concentrations and salt-nose extent for the dry period (6 ka).	56

## ACKNOWLEDGMENTS

This project was supported by National Science Foundation (NSF-EPSCoR).

I am deeply indebted to my advisor, Dr. Zhongbo Yu, for his constant support, persistence, and valuable guidance throughout my studies. Without his help, this work would not be possible. I would like to thank the members of my committee Dr. David Kreamer, Dr. Thomas C. Piechota and Dr. Ashok K. Singh for their advice, support and patience, and I would also like to thank Dr. Lambis Papelis for his continuous support during my studies.

I am very grateful to Dr. Weiquan Dong, who provided me invaluable support in groundwater recharge estimation using Maxey-Eakin method and groundwater model. Many thanks also to Liqiong Zhang who gave valuable help in computer related issues. I would like to thank my colleagues at University of Nevada Las Vegas, who helped and supported me in many ways over the years. Special thanks to Jon Wilson, Ryan Rowland and Ron Veley with U.S. Geological Survey Henderson, Nevada, for their support in both my study and work related matters.

Lastly, I would like to thank my family for their love and support.

## CHAPTER 1

### INTRODUCTION

#### 1.1 Introduction and Literature Review

Pilot Valley, part of the Great Basin and located in the western United States, is a tectonic trough and a hydrologically closed basin (Snyder, 1962). Snyder (1962) explained that water exits from the hydrologic system to the atmosphere through evapotranspiration within the closed basin. He used the term “undrained closed valley” where the area is “topographically and hydrologically closed” with no outlets except to the atmosphere through evapotranspiration. According to Duffy and Al-Hassen (1988), the existence of a closed basin can be verified by calculating mass balance or deficit between net inflow and outflow of water over a long period of time. They also mentioned that if there is a surplus on the water balance, there is no closed basin because additional water is coming to the system from other sources. Conversely, a deficit indicates leakage, which nullifies the idea of a closed system.

According to Langbein (1962), Pilot Valley has high annual evaporation that exceeds annual precipitation and has high content of salt accretion. He reviewed the classic explanation of accumulation of salt in closed basins, that is, the total salt load is thought to be the entire quantity of salt buildup during the time intervening since an open lake last overtopped the playa. According to Duffy and Al-Hassan (1988), salts do not

readily accumulate when a playa is dry with only occasional flooding, but in wetter conditions when the water table is high, salinity can readily increase due to the concentration of salts associated with evaporation. Also the gross physical character of the bedrock formation and nature of the sediment within the playa basin strongly affects saltwater chemistry (Rosen, 1994).

This study focuses on the groundwater and density driven flow in Pilot Valley's closed basin. Since all discharge from this basin occurs through evapotranspiration on or near the playa, the water table of the aquifer beneath the playa is often just below the ground surface (Duffy and Al-Hassan, 1988). According to McCleary (1989), Pilot Valley experienced diverse climatic conditions over thousands of years. Also, this variability of climate caused fluctuation of water table that subsequently affected the hydrogeochemistry of the playa. For example, near surface water table creates conducive environment for a density driven flow by dissolving the salt crust on the playa.

Using numerical simulations, Duffy and Al-Hassan (1988), demonstrated the presence of two types of flows, free convection flow and forced convection flow in Pilot Valley. As mentioned above, the former occurs due to the higher density of brine beneath the floors of closed valleys. The latter occurs due to a hydraulic gradient, when precipitation falls on the mountain side and percolates to the subsurface through fractured rocks, talus slopes and alluvial fans. This water undergoes forced convection then returns to the lower area or valley as springs, and drains into the playa.

The present study analyses the free convection flow and forced convection flow under variable climate conditions of the last glacier maximum (LGM), which induce differing groundwater recharge. Further, this study presents numerical experiments

designed to help understand the density driven groundwater flow in a closed basin (Pilot Valley) by addressing the following issues. First, the study determines the effect of climatic variability that induces different recharge values on the density driven groundwater flow. Second, the study analyzes the response in the groundwater flow and solute transport under variable geologic conditions (high and low permeability). Third, the study determines the scaling relationship that helps minimize the spatial difference of elevation in the study area.

## 1.2 Description of Study Area

### 1.2.1 Location

Figure 1.2 shows the Great Basin, which is part of the Basin and Range Physiographic Province. It is an internally draining basin that covers several States including most of Nevada and bordering areas of Utah, Oregon, Idaho, and California (Snyder, 1962). Pilot Valley, which is part of this basin, is located on the boundary between northeastern Nevada and northwestern Utah, and enclosed by two mountain ranges, Silver Island Range with altitude of 2,305 meters above sea level (asl) to the east and Pilot Range with altitude of 3,266 meters asl to the west (Fan et al., 1997). Also according to Fan et al. (1997), the valley floor is approximately 1,292 meter asl.

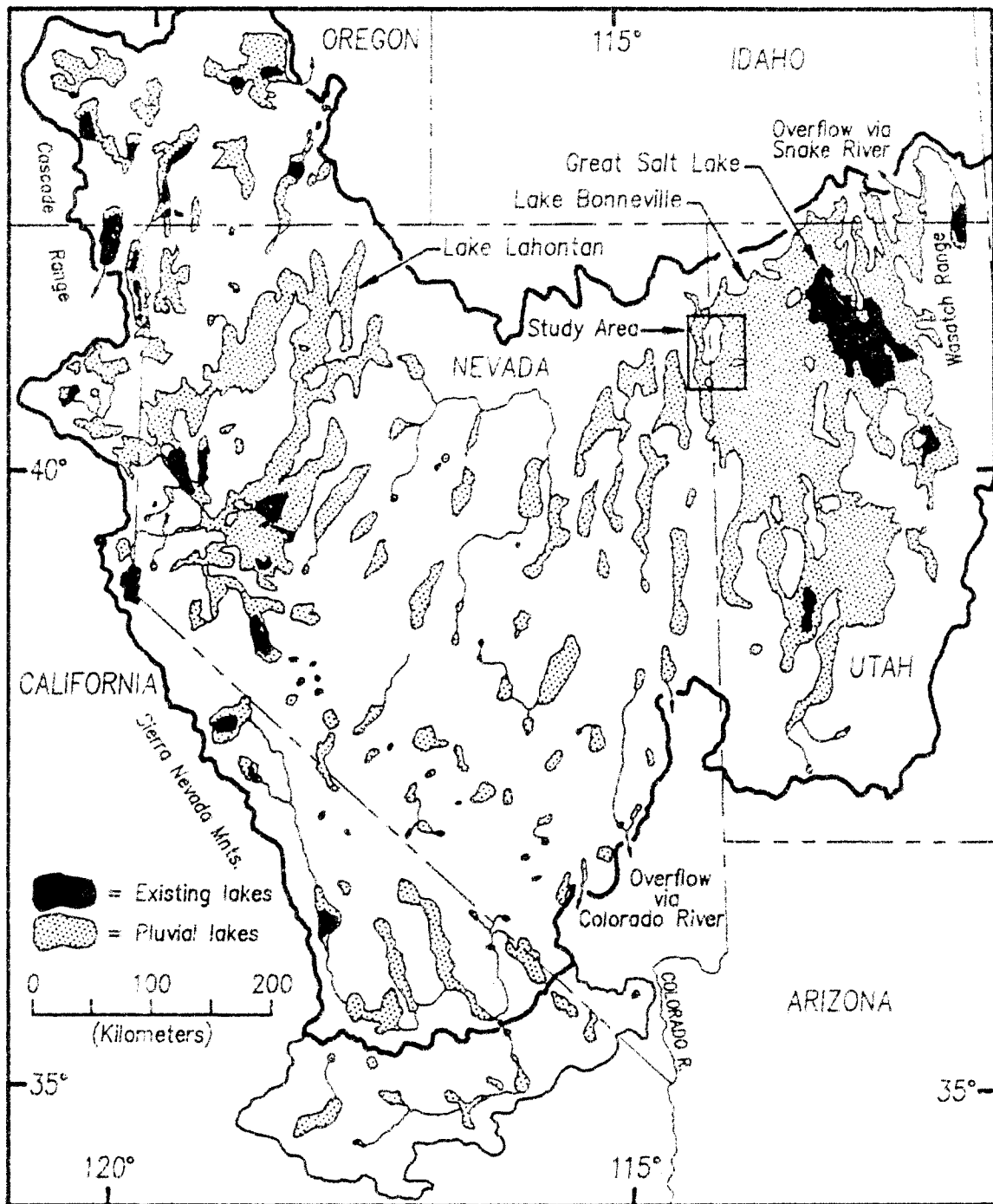


Figure 1.1 Extent of pluvial lakes, playa basins and existing salt lakes of the Great Basin  
(After Fan et al., 1997).

### 1.2.2 Geology

The geologic features of Pilot Valley and the Great basin as a whole are typified by parallel, north-south oriented mountain ranges that split areas of broad valleys and playas. These often have massive alluvial fans and flat valley floors (Lines, 1979; Fan et al., 1997). The structure of Pilot Valley which is part of the Great Basin has been described as a series of blocks, tens of miles wide that have been alternatively uplifted and depressed, resulting in folding and high-angle faults (Fenneman, 1931). According to Lines (1979), the mountain ranges of the study area are bounded on one or more sides by high-angle block faulting often having several thousands of feet of displacement, and basins filled with evaporites and material eroded from adjacent mountains. Furthermore, he explained that the study area is mainly composed of limestone, dolomite, shale, and quartzite of Paleozoic age (Figure 1.2).



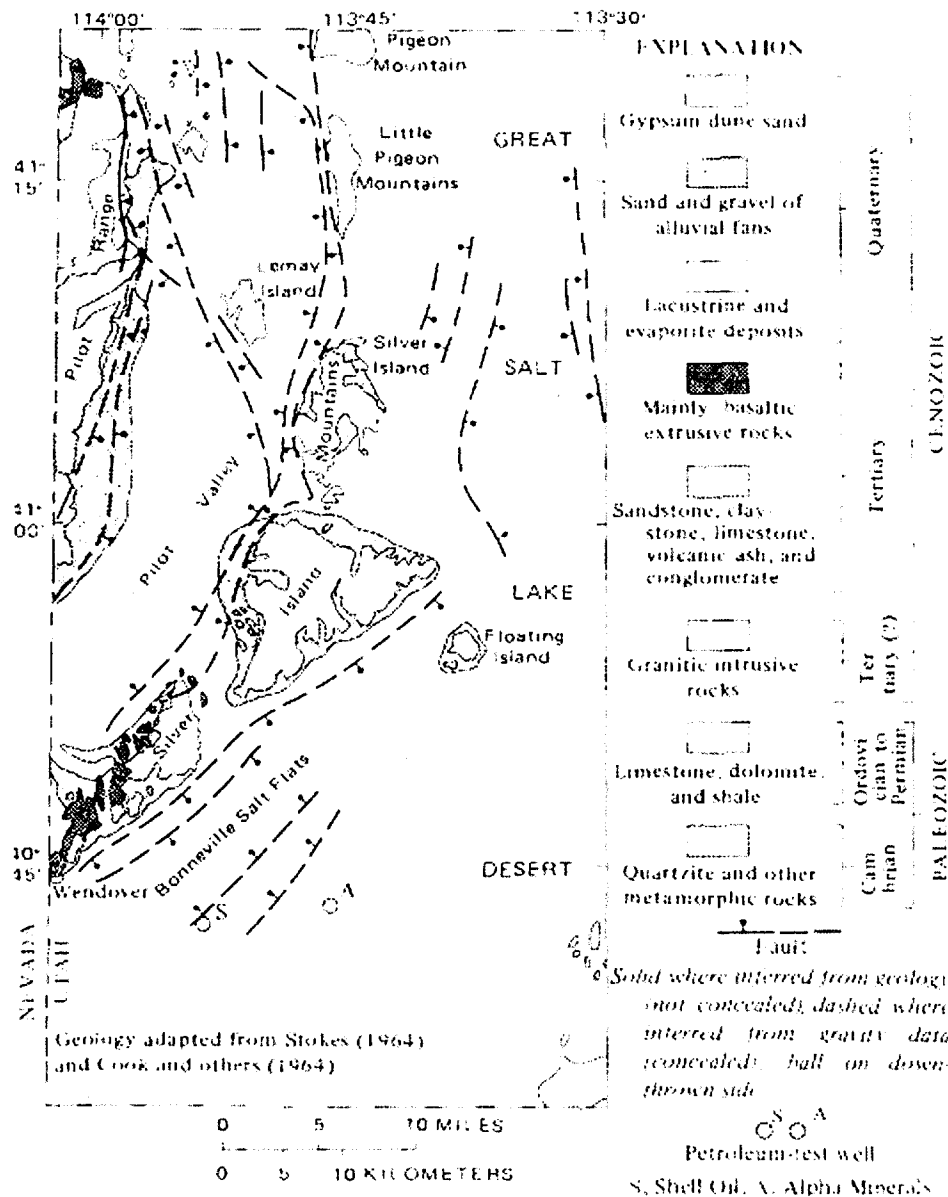


Figure 1.2 Geology of Pilot Valley and the Bonneville Salt Flats of the Great Salt Lake Desert (from Lines, 1979).

According to Fan et al. (1997), there are three geomorphic features that characterize a closed basin such as Pilot Valley. These features are: precipitous and craggy bedrock slopes higher up, underlain by massive alluvial fans, with extremely flat

valley floors and playas below. Moreover, because the study area lacks a surface outlet, the valley keeps all of the eroded materials originating from adjacent mountains, producing a markedly deep basin fill, which can be as thick as 3,000 m at places (Harrill et al., 1983). The basin fill above Paleozoic sedimentary rocks is classified by Fan et al. (1997) into four units (Figure 1.3). They are:

- Tertiary age colluvium and alluvium which are partially consolidated, overlain by
- Fine grained lacustrine, aeolian and alluvium of quaternary age which represent signatures of changing climatic periods and are interbedded, which underlie,
- The third unit, which is comprised surface carbonate muds and crystalline halite, and finally,
- The fourth unit comprised of alluvial fans and deep basin fill, which provide the main groundwater storage (Mason et al., 1998), and that thickly cover the mountain slopes and interfinger with the other three units.

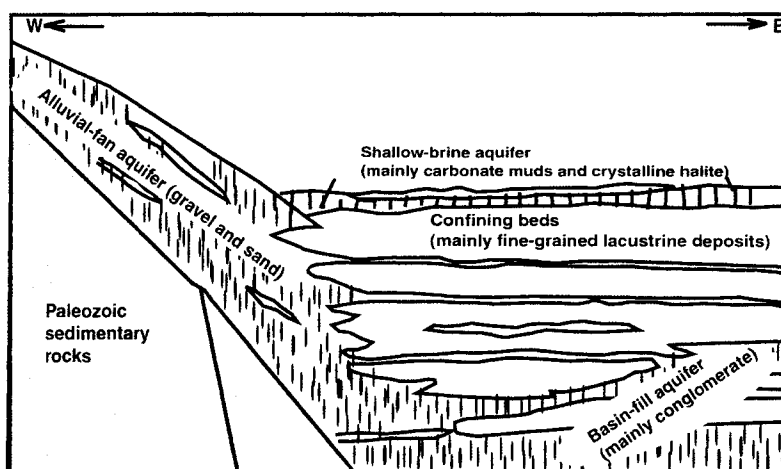


Figure 1.3 Stratigraphic relationships between four major geologic units of the Great Basin (from Lines, 1979).

According to Snyder (1962), large accumulation of carbonate muds and crystalline halites are produced by high evaporation rates in the broad playas of closed basins. Neal (1965) notes the presence of thrust polygons in this evaporative environment, on parts of the valley which are associated with rapid upward capillary movement of water. It is important to note, the deposition of surface salts is controlled by fluctuating water table in the playa. Above surface water table creates conducive environment for sediment deposition, conversely, lower water table, under the surface of the playa causes erosion of sediment (McCleary, 1989). This dynamic interaction between climate, hydrology, and the surface sediments or salts makes the study area “the flattest of all landforms” (Neal, 1965).

### 1.2.3 Climate and Hydrology

Pilot Valley and the Bonneville Salt Flats are located in the northeastern part of Nevada and northwestern part of Utah, which have similar hydrologic conditions (Lines, 1979). These areas are subjected to the temporal and spatial variability of climate (Fan et al., 1997). Strand lines, and other depositional evidences of ancient shorelines, chronicle the succession of past pluvial lakes in the basins (Fan et al., 1997). According to Morrison (1968), there was quite a difference in temperature and precipitation of Lake Bonneville during its high stage; that is, mean annual temperature was 3-5<sup>0</sup>C lower and precipitation was 180-230 mm higher than present. Further, the physiographic nature of the areas creates a wide spatial variability of climate, with annual precipitation ranging from 80 mm in the low level areas (playas) to 1,500 mm in surrounding mountain ranges, and annual mean temperature ranging from 33<sup>0</sup>C to 17<sup>0</sup>C (Fan et al., 1997).

Physiography exerts a profound influence on the movement of water in Great Basin. Duffy and Al-Hassan (1988) used numerical simulations to analyze the climate and topographic characteristics of the hydrogeochemistry of Pilot Valley. The study found that the orientation of the landform has a significant effect on the hydrology of the region. As described above, the mountains receive high precipitation and act as the main recharge areas but have little storage capacity, while the playa floor remains arid.

The process of groundwater flow in a closed basin accommodates two types of flow (Figure 1.3): forced (advective) flow and free convective flow (Duffy and Al-Hassan, 1988). Forced convective flow or advective flow occurs when precipitation falls on the mountain front, then percolates to the groundwater through the fractured rocks and returns to the surface as springs and drains to the playa, due to the absence of a subsurface outlet (Duffy and Al-Hassan, 1988; Doughty, 1999). Free convective flow occurs when a denser fluid is placed on top of a less dense fluid and the former sinks in order to achieve stability (Simmons, 2001). In the figure below, the denser fluid reaches the bottom of the basin fill, extends to the left, encounters and mixes with the freshwater in the forced convective path, flows upward after diluted, and returns to the playa surface. The water on the playa surface evaporates to the atmosphere and completes the ‘hydrologic cycle’ of a closed basin.

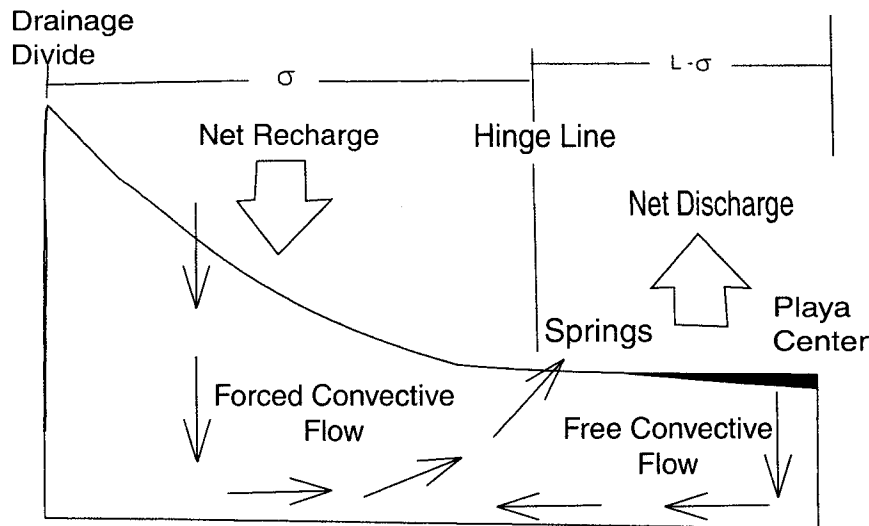


Figure 1.4 Conceptual model showing types of groundwater flow in a closed desert basin.

$\sigma$  and  $L-\sigma$  show the length of recharge and discharge areas respectively (from Duffy and Al-Hassen, 1988).

The hydrologic boundary or ‘hinge line’ (Figure 1.3), which is found on the margin slope and the playa is applied in the study. The hinge line defines the length scale of the recharge and discharge to the groundwater system. It is based on the study made by Toth (1962), and Fan et al. (1997), who conducted field studies and numerical simulations to examine the existence of this line.

### 1.3 Scope and Objectives

This study focused on analyzing the groundwater flow (presence or absence of free convection), and how climatic variability, geologic conditions, and scaling issues of Pilot Valley would affect the groundwater flow and solute transport. The specific objectives in this study are: (1) to implement the Saturated and Unsaturated Transport

model (SUTRA) for the hydrologic system of a closed basin (Pilot Valley); (2) to depict the response of hydrologic systems due to geologic variability; (3) to determine the scaling relationship of elevation and distance; and (4) to evaluate the response of groundwater flow and solute transport to the warming and drying climates in the past 20 thousand years (20 ka).

## CHAPTER 2

### METHODOLOGY AND MODEL SIMULATIONS

#### 2.1 Methods Associated with Factors Affecting Groundwater Flow in a Closed Basin

##### 2.1.1 Climatic Variability

The depositional remnants of past lake environments are contained in the stratigraphic records around the sites of historic lakes Bonneville and Lahontan (Morrison, 1968). These remnants show regional, climatically-induced depositional changes and contain sensitive, full, and easily available records of late Pleistocene conditions. Pilot Valley and the Bonneville Salt Flats, aside from providing not only qualitative data on the climatic change from geomorphic traces, also offer means of determining past temperature and precipitation values in a more quantitative way than is possible from most surficial geologic areas (Fan et al., 1997). Understanding past and future hydrologic systems requires an understanding of temporal and spatial climatic variability. Further, understanding the relationship between past climate and hydrology offers a basis for evaluating and predicting future change in the flow system.

Dong (2004) developed a coupled catchment-lake model that utilizes meteorological records (i.e., precipitation and temperature) and digital elevation models. It uses a climate circulation model and proxy data to derive paleoclimatic variability. The coupled catchment-lake model extracted quantitative paleoclimate information over the past 20 ka. Lake records from hydrologically closed basins in the Owens River Valley,

California, including Owens, China, and Panamint Lakes, and Death Valley, respond to water balances within their catchments and are sometimes expressed as “natural rain gauges” (Smith et al., 1997). Precipitation and temperature data obtained from this model compared well with the previously published data (Table 2.1).

Owens River Valley has hydrogeologic conditions comparable to those of the study area, and output of precipitation and temperature from this model, over the last glacier maximum (LGM), was used as input for this study.

Table 2.1 Proxy data in the southwest United States in the last 18 ka (Dong, 2004).

Time	Temperature (°C)	Precipitation	Source
18 ka	-3.29 annual -3.17 Jan, - 3.01 Jul	-0.29 mm/day annual +0.25 mm/day Jan, -0.84 mm/day Jul	Thompson et al., 1994
20.5 to 18 ka	-7.5 annual	2.40x	Thompson et al., 1999
14 to 11.5 ka	-6.7 annual	2.58x	Thompson et al., 1999
12 ka	-2.52 annual -3.01 Jan, - 0.63 Jul	-0.18 mm/day annual -0.27 mm/day Jan, -0.15 mm/day Jul	Thompson et al., 1994
9 ka	+0.43 annual -0.09 Jan, +2.15 Jul	+0.30 mm/day annual +0.80 mm/day Jan, -0.27 mm/day Jul	Thompson et al., 1994
6 ka	+0.69 annual +0.30 Jan, +0.68 Jul	-0.03 mm/day annual -0.16 mm/day Jan, +0.07 mm/day Jul	Thompson et al., 1994

The spatial variability of precipitation has an impact on groundwater flow and solute transport. The Maxey-Eakin method describes an empirical relationship between



elevation and precipitation, and is used to examine the spatial variability in precipitation. In this method, precipitation is estimated as a function of elevation (Table 2.2). A higher elevation yields higher precipitation and a lower elevation yields relatively lower precipitation. Further, the method helps distribute groundwater recharge values according to the elevation of the study area. The recharge is then used to drive the SUTRA model for assessing how the climate change would affect the groundwater flow and solute transport in this setting.

### 2.1.2 Geologic Heterogeneity

Geologic heterogeneity has an impact on the groundwater flow and solute transport (Wooding, 1978). It is associated with the presence of different geologic units, which exhibit different permeability values, along a geologic profile. Fan et al. (1997) conducted numerical simulations with different permeability values based on the setup in Figure 2.1. Further, their study assumed a decrease in the particle size towards the playa due to the downgrading of alluvium and sequence of cobble, gravel, sand and silt. Also, three layers of clay were embedded in the silt matrix and the fractured rock was treated as an equivalent porous media. The units are assigned permeability values that differ by five orders of magnitude. An arithmetic and harmonic mean of permeability were obtained for the horizontal and vertical layers respectively (Wooding, 1978), and applied uniformly in a simulation to represent an equivalent, homogeneous system. This value was very close to the permeability value of silt (Fan et al., 1997). The averaged horizontal and vertical permeability can be calculated with the following formulas (Bouwer, 1978):

$$k_x = \frac{\sum k_i d_i}{D} \quad (1)$$

$$k_z = \frac{D}{\sum \frac{d_i}{k_i}} \quad (2)$$

Where  $D$  is the total depth of the system,  $d_i$  is each individual layer's thickness, and  $k_i$  corresponds to layer's permeability. Both vertical and horizontal permeabilities are assigned an overall effective permeability (Maasland, 1957).

$$k_r = (k_x k_z)^{0.5} \quad (3)$$

Where  $k_r$  is effective permeability.

This effective permeability value is used in the SUTRA model in this study for different time periods (Modern, 6 ka, 9 ka, 12 ka, 15 ka, and 18 ka).

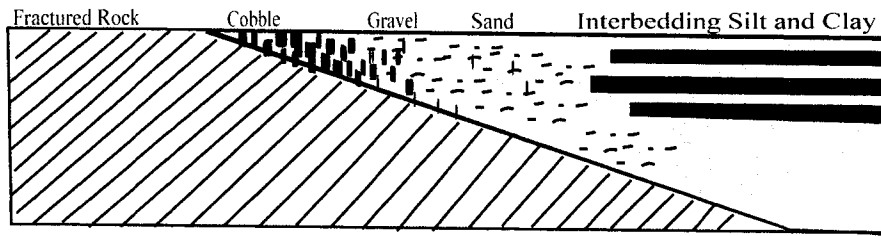


Figure 2.1 Heterogeneity of the basin-scale aquifer resulting in different permeability values (after Fan et al., 1997).

### 2.1.3 Scaling Issue

The orographic effect over the great elevation range in the study area produces a strong gradient of temperature and precipitation from valley floor to mountain peaks (Fan et al., 1997). The Maxey-Eakin method (1949) is used to depict the spatial distribution of precipitation with a change in relief. The method which is an empirical relationship between elevation-precipitation-recharge has been widely used in Nevada and other

western regions. Avon and Durbin (1994) concluded that the Maxey-Eakin method was the best developed method to that time for recharge estimation in the Great Basin. For the specific application herein, precipitation and temperature have been analyzed using the Maxey-Eakin method in order to define the spatial difference of climatic variability. However, the Maxey-Eakin method alone does not sufficiently identify the scaling relationship. Therefore, by taking actual dimensions and topography of Pilot Valley an attempt was made to construct a generalized relationship for elevation versus distance. The contours in Figure 2.3 show the change in elevation and distance between the playa and divide. These changes in distance and elevation between the divide and the playa were used to normalize the individual slopes and spatially distributed elevation along the length of the study area. This scheme is called incomplete beta function (Duffy and Al-Hassan, 1988) and was incorporated in the study.

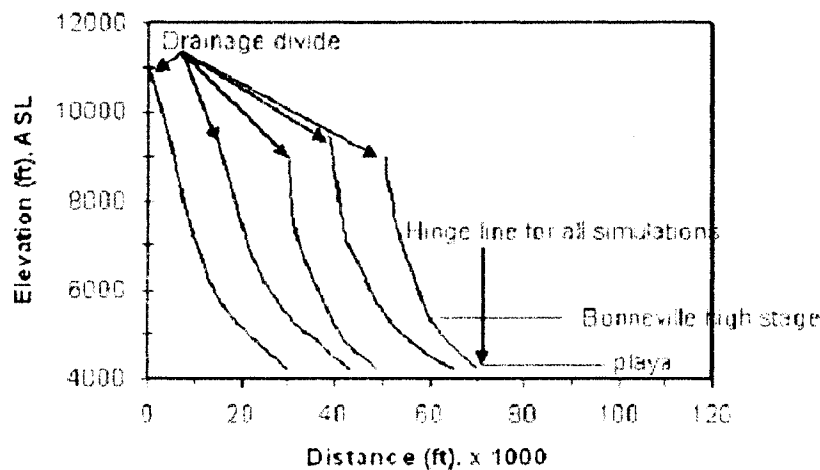


Figure 2.2 Elevation profiles versus distance from the playa to the mountain divide for the study area (data taken from U.S. Geological Survey topographic contour maps) (Duffy and Al-Hassan, 1988).

This function is compiled in a FORTRAN program. It yields a length of 13, 000 meters and elevation value of 1,300 meters for the entire recharge area described by nodes from the divide to the 'Hinge Line'. This scaling relationship is assumed to fit reasonably well for the Pilot Valley (Duffy and Al-Hassan, 1988), and would help distribute the net flux for each specified node along the recharge area.

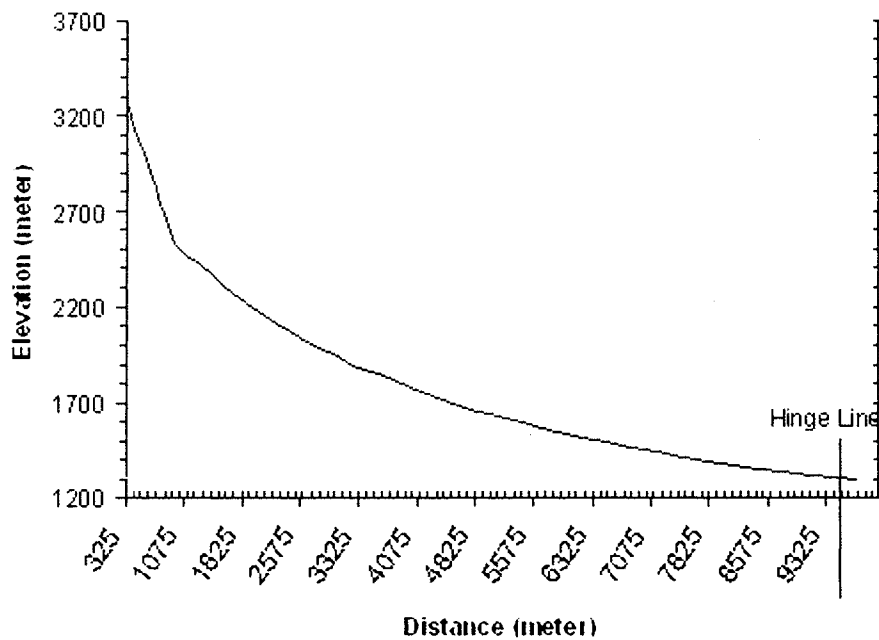


Figure 2.3 Normalized scaling relationship of elevation-distance from the incomplete beta function program.

#### 2.1.4 Groundwater Recharge Estimation and Saline Concentration Distribution

Natural groundwater recharge mainly occurs through precipitation. Thorough understanding of the spatial and temporal variability in precipitation could yield good estimations of recharge over long periods of time (Simmers, 1997). Groundwater moves from high mountain areas to lower areas at a low pace, commonly at rates ranging from a

small fraction to several hundred feet per year, depending on the geology of the deposits and the hydrology of the area (Simmers, 1997). The natural groundwater recharge tends to equilibrate with the groundwater discharge over an extended period of time. As described in previous sections, most recharge in Pilot Valley is provided by precipitation in mountain areas, with the water reaching lower areas by seepage loss from streams on the alluvial slopes and by underflow from consolidated rocks. As mentioned above, most of the precipitation evaporates before it infiltrates and only a small percentage of the precipitation becomes the natural groundwater recharge in an area. Precipitation is generally assumed to increase with elevation, and the portion of water reaching the groundwater reservoir is assumed generally to increase with precipitation.

Saline concentration is defined as the total mass in kilograms of all dissolved substances per kilogram of water. Pilot Valley and closed basins in general have various degrees of salinity, and this saline concentration is controlled by evaporation rate, groundwater salinity and density, hydraulic conductivity of the aquifer, and depths of near surface groundwater zones (Duffy and Al-Hassan, 1988). These depths of near groundwater zone have an effect on the variation in water density by activating convective and advective flows to balance the salinity gradient. According to Langbein (1961), the saline concentration fluctuates through time, and some evidence suggests that there is a substantial imbalance of salt since the appearance of the closed basin/lake, with less salt in a lake solution than the total input of salt into the lake through time.

#### 2.1.4.1 Groundwater Recharge Estimation Using Maxey-Eakin Method

Groundwater recharge moves in the direction of hydraulic gradient, that is, from higher to lower hydraulic head, under the pressure of gravity (Simmers, 1987). Recharge

is very critical in evaluating groundwater flow and solute transport and it is required as an input for the SUTRA model for this study. The recharge values differ from place to place. Therefore, quantifying and understanding its spatial distribution are very important for optimizing the significance of SUTRA model.

Groundwater recharge estimation can be based on a wide variety of models which are designed to represent the actual physical processes. This study uses the Maxey-Eakin method to estimate groundwater recharge. For a given altitude zone, a particular increment of total precipitation potentially recharges the groundwater reservoir. According to Avon and Durbin (1994), the method developed a relationship of elevation, precipitation and recharge by estimating annual precipitation for different watersheds, subtracting this annual precipitation from loss through evapotranspiration and runoff, and using the remainder to get the total groundwater recharge.

Table 2.2 Recharge coefficient distribution based on Maxey-Eakin method (from Duffy and Al-Hassan, 1988).

Elevation	Precipitation	Maxey-Eakin Recharge Coefficient (%)
>9000 ft.	>20 in.	25
8000-9000 ft.	15-20 in.	15
7000-8000 ft.	12-15 in.	7
6000-7000 ft.	8-12 in.	3
<6000 ft.	< 8 in.	0

The method is based on the empirical relationship between elevation and precipitation, and this link depends on the geography and climatic condition of an area. However, estimating groundwater recharge is, of course, dependent upon a large number

of factors including, but not limited to, latitude-longitude, proximity to coastal areas, topographic orientation (leeward or windward), vegetative cover, lithology, wind speed and solar radiation. Therefore, investigating true recharge efficiency would be a prolific research area for future scientists, but it is beyond the scope of this study.

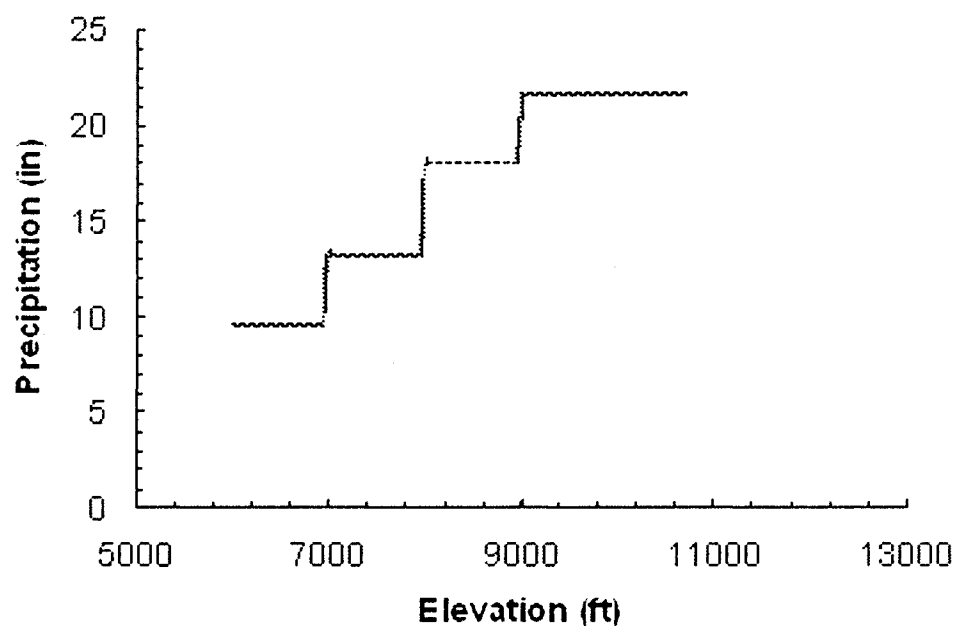


Figure 2.4 Modern precipitation distributions versus elevation based on Maxey-Eakin method (data from Appendix 1).

Using the elevation previously reported in this paper, a distribution of altitude is generated from a digital elevation model for Pilot Valley and surroundings (Figure 2.6). This distribution is used to produce the modern recharge value based on Maxey-Eakin method.

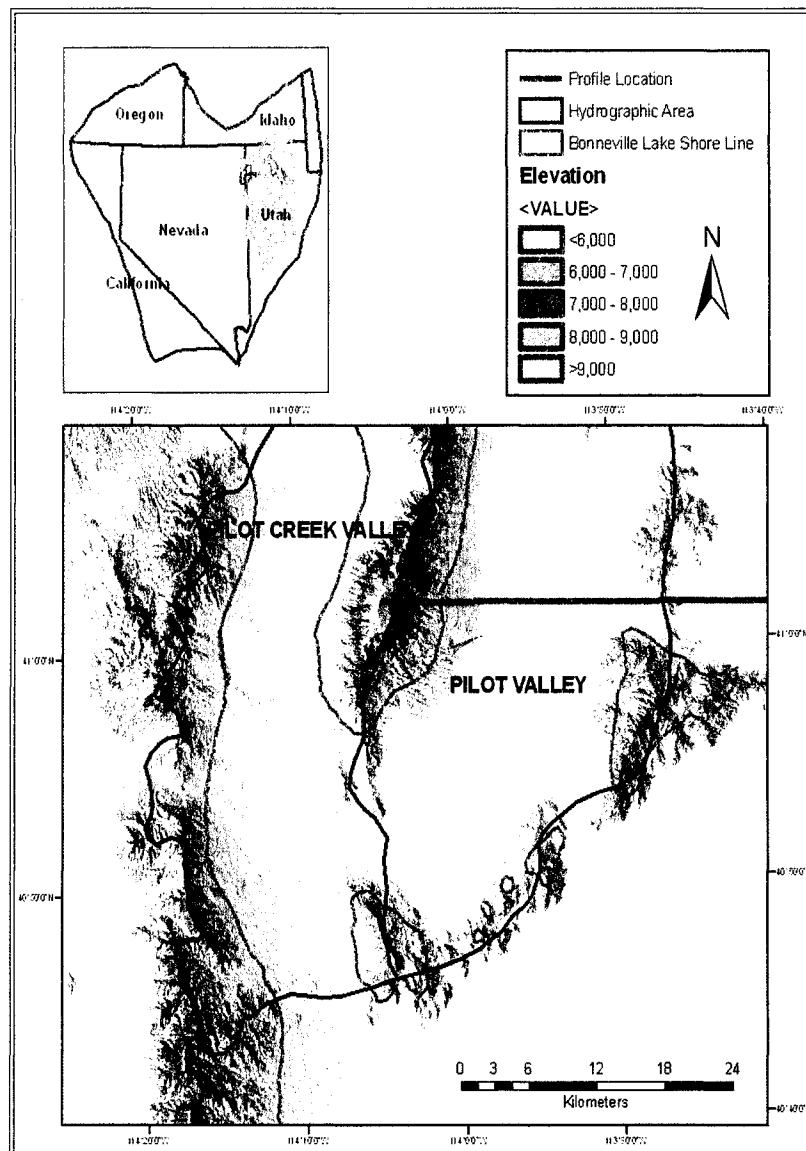


Figure 2.5 Elevation distributions and approximated profile location of the study area - Pilot Valley.

Aridity index was applied to assist in estimating groundwater recharge and this index was used to spatially average climatic factors such as precipitation and temperature. This index is a ratio between mean annual precipitation and mean annual



temperature. Additionally, the aridity index is a combination of Lang's index and a method by E.de Martonne (Ranjan et al., 2005).

The aridity index is defined by:

$$AI = \frac{P}{T + 10} \quad (4)$$

Where, AI = aridity index, P = mean annual precipitation (mm), and T = mean annual temperature (°C)

A flow domain (numerical grid) is developed based on the conceptual model (Figure 1.4) and recharge is specified to the top left side of the domain which is the mountain front recharge area. The Maxey- Eakin method, with coupled catchment-lake model and aridity index, helped distribute the modern recharge for the model. As described in Maxey-Eakin method, higher elevation gives higher recharge value. The boundary condition of the mountain recharge is specified, with the flow along the boundary varying spatially. The recharge values are incorporated to the BCTIME subroutine of the main program in the SUTRA model.

#### 2.1.4.2 Saline Distribution

Pilot Valley, a closed basin characterized by high evaporation and salinity (Fan et al., 1997). As previously mentioned in this paper, the unique chemistry, geology and physiography condition which reflect the local hydrology of the study area, respond sensitively to climatic change. Snyder (1962) explained that Pilot Valley is characterized by shallow brine with salt crust or wet mud surface. According to Rosen (1994), Pilot Valley is a closed basin characterized by near surface groundwater flow for extended period of time and this creates salt beds to great depths. Also, these salt beds play a major role in establishing the hydrogeochemistry of the flow system. As mentioned in the

preceding sections, this composition of the playa sediments mainly comes from the underlining and surrounding rocks of the drainage basin. In other words, the origin of brine water was thought to be the function of solute supply and salt concentration on the playa surface (Rosen, 1994). However, the groundwater flow system of two chemically different inflows is controlled by hydrologic settings and processes. These two inflows are the fresher water from the mountains area, which comes from precipitation that percolates to the ground through fractured rocks and denser fluid that flows in the reverse hydraulic gradient due to the high salt concentration in the Playa side.

Pilot Valley as described above is characterized by high evapotranspiration which consequently affects the concentration of solutes near the surface and causes density difference that further reverses the upwards hydraulic gradient, allowing the possibility of the advective reflux brines to the underling aquifer. Barnes et al. (1990) found in their model that advection is more important than diffusion in areas of high evaporation and recharge in transporting salt downwards. Hydrologic modeling of closed basins can provide calculated estimates of parameters in addition to actual observations. For example, Langbein (1962) described the possibility of modeling salt imbalance in a closed basin by having known geometric and physical parameters.

A transient saline concentration is prescribed from fresh lake water which changes from  $c=0.0003$  to  $0.2003$  ( $\text{kg kg}^{-1}$ ) over 5 ka from the beginning of the simulation (Fan et al., 1997) and this is applied in this study. The distribution of concentration follows a parabolic distribution (Figure 2.7) showing most rapid changes in concentration at early times in the simulation and eventually reaching a constant value of  $c=0.2003$  at 5,000 years. According to Morrison (1968), this distribution pattern of salt is

based on the estimation of what took place during the drying stage of Lake Bonneville. It is done by rebuilding the lake stage at the end of Pleistocene. The distribution was incorporated in the subroutine (BCTIME) of the SUTRA model.

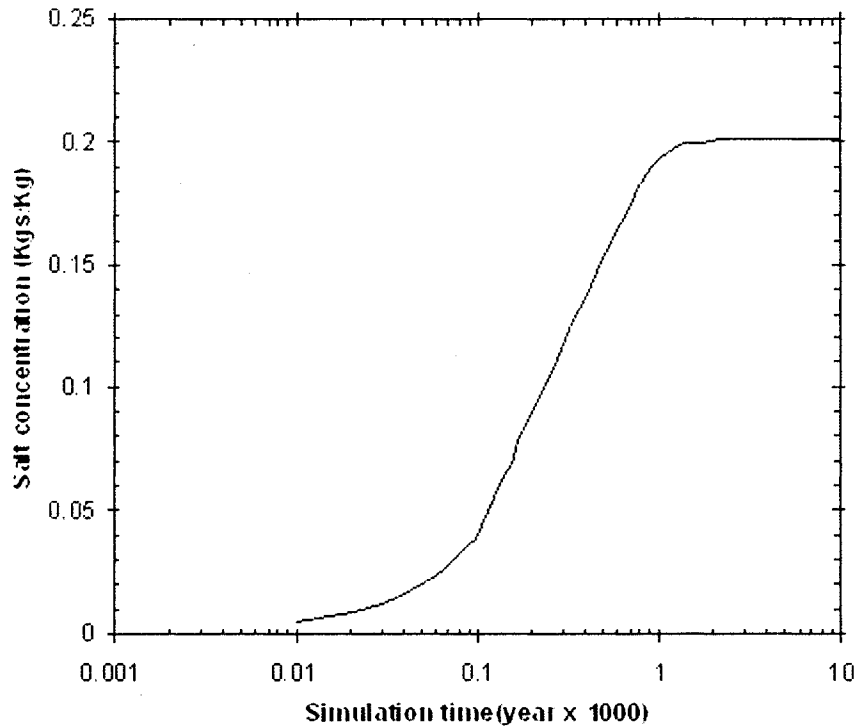


Figure 2.6 Parabolic distribution of saline concentration through time along the specified concentration nodes, based on the notion of the reconstructed Lake Bonneville stage at the end of Pleistocene.

## 2.2 Saturated and Unsaturated Transport Model (SUTRA)

Many of the assumptions in SUTRA model are obtained from the general observations made of physical phenomena in the field. For example, precipitation falling on the mountain ranges enters the groundwater system through fractured rocks and alluvial fans (Doughty, 1999; Pruess et al., 1999). The groundwater returns to the surface

as springs or drains into the playa. As mentioned above, the precipitation that falls within the basin feeds back to atmosphere through evapotranspiration from playa. The changes in groundwater flow system due to the climatic variability provided the background for constructing the conceptual model for this study, and the constructed model was used to simulate how the system responds to past and future climate changes. The hydrologic simulation for this study includes data compilation and analysis, implementation of SUTRA model, and Maxey-Eakin method with coupled catchment-lake model and aridity index.

The SUTRA model is one of groundwater models which have been applied to investigate a wide variety of hydrologic conditions. The SUTRA model examines the groundwater flow and solute transport through unified equations, and can simulate the fluid density dependent saturated or unsaturated groundwater flow and solute transport in the groundwater. In this study, saturated fluid density flow is crucial. The model also provides a calculated result for fluid pressure and solute concentration, as they vary with time everywhere in the simulated subsurface system.

The SUTRA model is based on a combination of finite element and finite difference methods applied in a fundamental structure of a scheme of “weighted residuals” (Voss, 1984). Both finite-element and finite-difference methods use partial differential equations which apply in governing equations, boundary conditions, and initial conditions and transform them in a way that can be understood and resolved by a computer (Anderson and Woessner, 1992). The application of SUTRA model with its finite element and finite difference methods is precise and strong enough to withstand challenges when implemented with appropriate spatial and temporal assignments of

discrete values (Voss, 1984). Voss also mentions that normal finite element estimations are utilized just for fluid and solute inflows or outflows and energy values, which are in the balance equation. However, the remaining terms that are not related to inflows and outflows of fluid, solute, and energy are approached by “a finite-element mesh version of the integrated finite-difference methods”. Additional software is used in this study, which includes Argus One, SutraPlot and model viewer. They are used for the pre and post processing and also help analyze and understand a conceptual model for the problem domain (grid size).

#### 2.2.1 Model Processes

SUTRA model can simulate groundwater flow and solute transport in two or three spatial dimensions (Voss, 2002). He further clarified that two dimensional flow may be done either in the areal plane or in the cross sectional view. Also groundwater flow is simulated through the numerical solution of a fluid mass balance equation and solute transport is simulated through the numerical solution of a solute mass balance equation where solute concentration may affect fluid density.

The model can simulate groundwater flow under saturated, or partly or completely unsaturated. In the SUTRA model, characteristics of fluid density are a function of solute concentration or fluid temperature. Furthermore, it incorporates specified sources and boundary conditions of fluid, and solute to vary with time.

#### 2.2.2 Model Application and Example

According to Voss (2002), the SUTRA model can be employed for groundwater flow and solute transport with a steady state condition which has one solution step, or transient that requires many time steps to obtain the calculated solutions. As discussed

above, the model could employ for two dimensional areal, cross sectional, and fully three dimensional modeling of saturated groundwater flow systems and unsaturated groundwater flow. Some of its application includes (Voss et al., 2002):

- Analysis of aquifer tests using flow simulation
- Restoration of groundwater contamination
- Understanding of seawater intrusion
- Simulation of thermal regimes in aquifers
- Understanding of variable density flow in different aquifers

Voss et al. (2002), showed as an example of Henry's problem which involves advances of a diffused salt-water wedge in a confined aquifer initially filled with freshwater. A constant rate of freshwater from the inland boundary mixes with encroaching water and exits to the ocean through the coastal boundary. This simulation is a typical case of variable density flow and studied in cross section under steady state conditions. According to Voss (2002), the boundary conditions for the flow equation consist of impermeable boundaries along the top and bottom of the rectangular aquifer, and hydrostatic pressure along the vertical boundaries (Figure 2.8). The concentration gradient is zero along the top, bottom, and the inland boundary; however, it is equal to the seawater concentration along the coast boundary.

Table 2.3 Physical parameters for Henry 1964 simulation solution (Voss et al., 2002).

Parameter	Unit	Value
Total time	Min	100
Time steps	-----	100
Mesh size (number of nodes)	-----	231
Mesh size (number of elements)	-----	200
Density of freshwater	$\text{kgm}^{-3}$	1000
Density of seawater	$\text{kgm}^{-3}$	1024.99
Initial concentration	$\text{kg}\text{kg}^{-1}$	0.0
Concentration of seawater	$\text{kg}\text{kg}^{-1}$	0.0357
Density coefficient	$\text{kg}\text{s}^2(\text{kgm}^3)^{-1}$	700
Recharge source	$\text{kg}\text{s}^{-1}$	0.066
Permeability	$\text{m}^2$	$1.020408 \times 10^{-9}$
Porosity	-----	0.35
Gravity	$\text{m}(\text{s}^2)^{-1}$	9.8
Dispersivity (longitudinal & transverse)	m	0

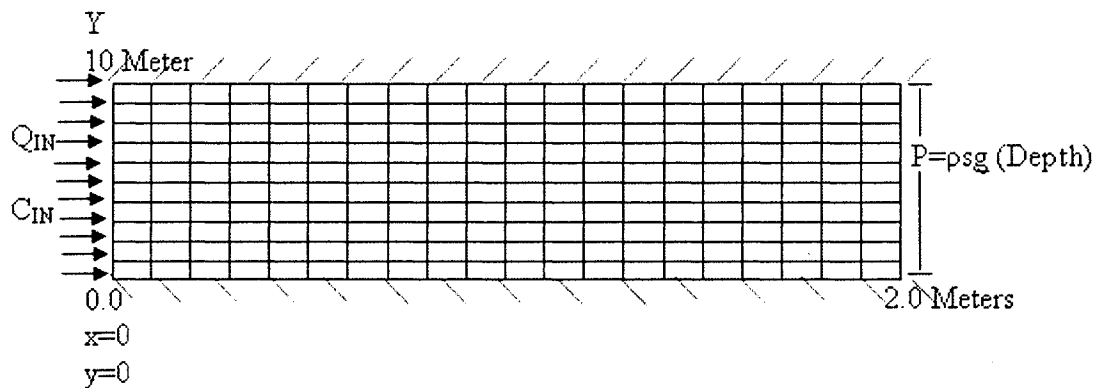


Figure 2.7 Finite element mesh and boundary condition for Henry 1964 solution

(From Voss et al., 2002).

Saltwater intrusion is common when the salinity of a surface water body is higher than the salt content of the natural groundwater. Domenico (1972), explained this condition by saying that demands for subsurface freshwater and its consequent depletion creates an imbalance between freshwater and seawater, and this promotes the intrusion of

salt water into the utilizable freshwater aquifer. From the result in Figure 2.9, one could conclude that a dispersion zone built up from the salt water boundary into the freshwater zone and made its way up to the upper surface and then followed its normal course. The reason is that the saltwater wedge at the bottom of a unconfined aquifer may move long distances against the hydraulic gradient and the driving force for this phenomenon is the higher density of saline fluid in comparison to fresh water (Holzbecher, 1998).

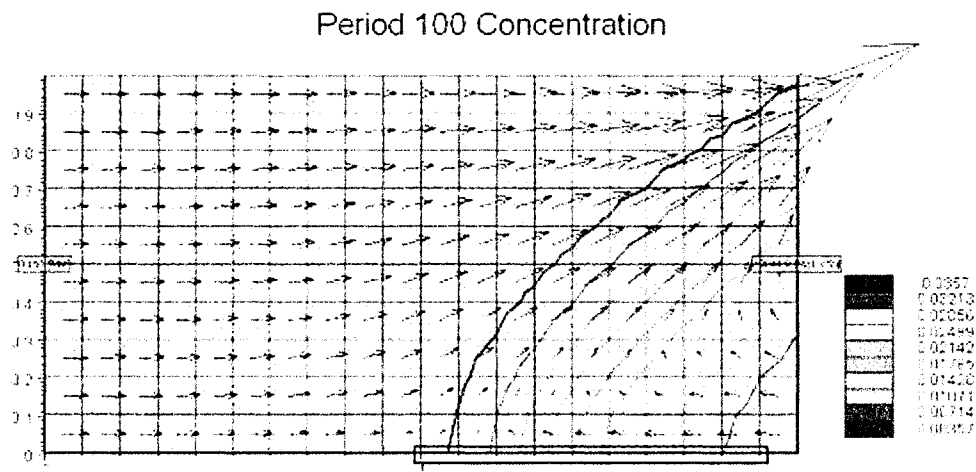


Figure 2.8 Simulated velocity fields and salt concentrations for Henry 1964 (Legend shows salt concentration in  $\text{kg/kg}^{-1}$  units).

### 2.2.3 Model Parameters for Study Area

Appropriate boundary and initial conditions are very important to accurately represent the hydrogeology of the system. According to Fan et al. (1997), the hypothesis of assigning the left and right no flux boundary conditions (Figure 2.9) is based on the assumption that mountain ranges and the valley are symmetric about their north-south orientations in the Great Basin. Their hypothesis applies also for the bottom no flux



boundary and it is based on the general geology of the Great Basin which indicates a basin fill underlain by consolidated Precambrian sedimentary rocks (Figure 1.3). The left top side of the numerical domain (Figure 2.9), is a specified boundary condition where a freshwater percolates into the system. The net flux for this study herein distributes along the boundary based on the Maxey-Eakin method with coupled catchment-lake model and aridity index. Also, the right top side of Figure 2.9 which is a discharge area, describes a specified pressure with  $p=0$ , showing a saturated condition or shallow groundwater and also it has a specified concentration with  $c=c_1(t)$ . These specified boundary conditions are incorporated in the subroutine of the SUTRA program. A two-dimensional cross sectional view, with spatial Cartesian  $(x, y)$  coordinate is applied. It is a transient system with the density dependent flow.

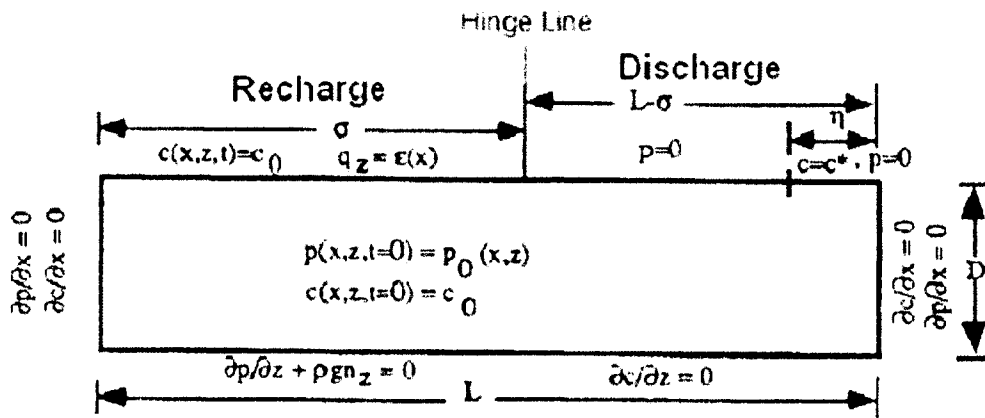


Figure 2.9 Mathematical representation of the conceptual model with its boundary, geometry and initial conditions (from Duffy and Al-Hassan, 1988).

The field parameters (Table 2.4) are assigned with a particular value in each element of a finite-element mesh or are assigned with a particular value at each node in

the mesh in either nodewise or cellwise (Figure 2.10). For example, the discretizations of permeability and porosity are elementwise and nodewise assignment respectively.

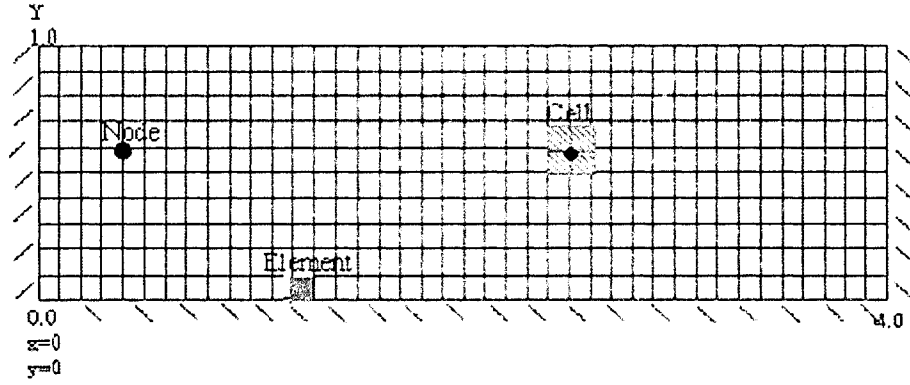


Figure 2.10 Finite-element grid used in half-basin simulation (41\*11 arrays of nodes) and cell, element and nodewise discretization for a two-dimensional finite element mesh.

According to Voss et al. (2002), SUTRA assigns discrete values for the physical parameters based on node, element or cell (Figure 2.10). For example, equation that yields the elementwise discretization for hydraulic conductivity is:

$$K(x, y) \approx \sum_{L=1}^{NE} K_L(x, y) \quad (5)$$

Where, NE = total number of elements in the mesh,  $K_L(x, y)$  [L/s] = the value of hydraulic conductivity of element L for (x, y), coordinates within the element, and a value of zero outside the element,  $K(x, y)$  = represented in a discrete approximate way by the sum of all the “boxes”.

Meanwhile, the hydraulic head distribution in two dimensions could be described with equation (Voss, 2002):

$$h(x, y, t) \approx \sum_{j=1}^{NN} h_j(t) \phi_j(x, y) \quad (6)$$

Where, NN = total number of nodes in the grid size,  $h_j(t)$  = hydraulic flux with time at the cartesian coordinates  $(x_j, y_j)$  of node number  $j$ ,  $\phi_j(x, y)$  is identified as the “basis function”

Cellwise discretization was also explained in the SUTRA model for the two dimensional system for the storativity parameter (Voss, 2002).

$$S_o(x, y) \approx \sum_{i=1}^{NN} S_i(x, y) \quad (7)$$

Where, NN = total number of nodes,  $S_i(x, y)$  = value of specific storativity of the cell centered on node  $i$  for  $(x, y)$  coordinates within the cell, and a value of zero outside the cell,  $S_o(x, y)$  = represented in a discrete, approximate way by the sum of all the “boxes”.

The simulation domain used to define the location of the nodes and elements for the half basin case is consistent with previous studies done in the study area (Duffy and Al-Hassan, 1988; McCleary, 1989; Fan et al., 1997). Further, the study area has a length of 13,000 by 1,300 meter depth, with aspect ratio of 10 (i.e., L/D) (Table 2.4). Thus, the simulation geometry was divided into rectangular elements made up of 41 by 11  $(x, y)$  nodes (Figure 2.10) and this geometry represents the study area well.

#### 2.2.4 Numerical Method for the Simulation of Fluid and Solute Transport

Numerical methods are employed to represent the subsurface groundwater flow and solute transport. Rayleigh number is a parameter, which is used to define the presence of free convection in the system (McCleary, 1989; Smith et al., 2001).

According to Duffy and Al-Hassan (1988), the buoyancy and resistant forces in terms of velocities can be expressed by

$$Ra = \frac{\left[ \frac{k \Delta \rho g / \mu}{\varepsilon} \right]}{\left[ \frac{\alpha_T}{L} \right] \left[ \frac{L}{D} \right]} = \frac{\left[ \frac{\text{Buoyancy velocity}}{\text{Recharge velocity}} \right]}{\left[ \frac{\text{Despersive length scale}}{\text{System length scale}} \right] [\text{Aspect ratio}]} \quad (8)$$

Where  $k$  is mean intrinsic permeability  $\{l^2\}$ ,  $\Delta \rho$  is density contrast between recharge and discharge fluids  $\{m/l^3\}$ ,  $g$  is gravity  $\{l/t^2\}$ ,  $\mu$  is dynamic viscosity  $\{m/lt\}$ ,  $\varepsilon$  is mean recharge rate  $\{l/t\}$ ,  $\alpha_T$  is transverse dispersivity  $\{l\}$ ,  $D$  is depth of the basin  $\{l\}$ , and  $L$  is length of the basin  $\{l\}$ .

A general form of Darcy's law, which is commonly used to describe the flow in porous media, expresses the mechanism of pressure and density-driving forces for flow (Voss, 1984).

$$V_i = -\frac{k_{ij}}{\phi \mu} \left( \frac{\partial P}{\partial X_j} - \rho \left( -g \frac{\partial Z}{\partial X_j} \right) \right) \quad (9)$$

Where  $V_i$  is the average fluid velocity  $\{l/t\}$ ,  $k_{ij}$  is the permeability tensor of porous medium  $\{l^2\}$ ,  $P$  is fluid pressure,  $\phi$  is porosity,  $g$  is gravity  $\{l/t^2\}$ , and  $\partial z / \partial x_i$  is the hydraulic gradient.

The SUTRA model calculates how fluid mass within the void spaces in a control volume changes with time. The fluid mass balance can change due to inflow or outflow, change in velocity or density, or sources and sinks within the control volume. It can be expressed as (Voss, 1984):

$$\frac{\partial(\rho \phi)}{\partial t} = -\frac{\partial}{\partial X_i} (\phi \rho V_i) + Q_p \quad (10)$$

Where the term on the left hand side may be recognized as the total change in fluid mass contained in the void space with time. The first term on the right hand side represents the contributions to the local fluid mass change due to excess fluid inflows over outflows at a

point. The last term associated with fluid source that includes fluid and solute mass. For a saturated condition, the total change in fluid mass contained in the void space with time is defined by (Duffy and Al-Hassan, 1988):

$$\frac{\partial(\rho\phi)}{\partial t} = (\rho S_{op}) \frac{\partial P}{\partial t} + \left( \phi \frac{\partial \rho}{\partial c} \right) \frac{\partial c}{\partial t} \quad (11)$$

$S_{op} = (1 - \phi)\alpha + \beta\phi$ , which the specific pressure storativity is zero for incompressible fluid and porous medium; so it eliminates the first term. Where  $\alpha$  is matrix compressibility  $\{1t^2/m\}$ , and  $\beta$  is fluid compressibility  $\{1t^2/m\}$ :

$$\frac{\partial(\rho\phi)}{\partial t} = \left( \phi \frac{\partial \rho}{\partial c} \right) \frac{\partial c}{\partial t} \quad (12)$$

Hydrodynamic dispersion is one of the mechanisms that transport solute mass by both mechanical dispersion and molecular diffusion. The SUTRA model defines solute dispersion in the form of anisotropic dispersivities. The dispersion tensor is represented as (Voss, 1984):

$$D_{ij} = \begin{bmatrix} D_{xx} & D_{xz} \\ D_{zx} & D_{zz} \end{bmatrix} \quad (13)$$

Where  $D_{xx} = (1/v^2) (\alpha_L v v_x^2 + \alpha_T v v_z^2)$ ,  $D_{zz} = (1/v^2) (\alpha_T v v_x^2 + \alpha_L v v_z^2)$ , and

$$D_{xz} = D_{zx} = (1/v^2) (\alpha_L v - \alpha_T v) (v_x v_z)$$

Where  $\alpha_L$  is the longitudinal dispersivity of solid matrix  $\{1\}$ ,  $\alpha_T$  is the transverse dispersivity of solid matrix  $\{1\}$ ,  $v$  is the magnitude of velocity  $v_i$ ,  $v_x$  is the magnitude of x-component of velocity  $v_i$ , and  $v_z$  is the magnitude of z – component of velocity  $v_i$ .

The transverse and longitudinal dispersivities are independent of the flow direction and are considered as fundamental properties of the system.

The solute mass balance for a system in which there are no adsorption/desorption, production/decay, or dissolution/precipitation reactions is defined as (Voss, 1984):

$$\frac{\partial(\rho\phi c)}{\partial t} = -\frac{\partial}{\partial X_i}(\phi\rho V_{ic}) + \frac{\partial}{\partial X_i} \left[ (\phi\rho(D_m\delta + D_{ij})) \frac{\partial c}{\partial X_j} \right] + Q_p c^* \quad (14)$$

Where  $D_m$  is the apparent molecular diffusivity of solute in solution in a porous medium including tortuosity effects [ $L^2/s$ ],  $D_{ij}$  is the dispersion tensor [ $L^2/s$ ],  $\delta$  is the identity tensor [ $L$ ], and  $c^*$  is the solute concentration of fluid sources (mass fraction) [ $Ms/M$ ].

The left hand side term of the above equation shows the total change of solute mass in the saturated volume with time. The first term of the right hand side describes the average advection of solute mass into or out of the local volume. The second term of the right side defines the contribution of solute mass from diffusion and dispersion processes. The final term shows the solute mass added to the system by the prescribed concentration of the fluid source.

#### 2.2.5 Physical Parameters

The idealized mathematical representation of the conceptual model (Figure 2.9) illustrates a homogeneous condition. The study area is assumed to be symmetric, and only half of the basin is simulated. The recharge zone corresponds to the zone between the mountain divide and the hinge line for the simulations. The physical parameters are important to accurately simulate groundwater flow and solute transport. Most of the parameters are obtained from previous studies conducted in Pilot Valley and mainly from the studies of Lines (1979), Duffy and Al-Hassan (1988), McCleary (1989), and Fan et al. (1997). Porosity and permeability values are typical for silt under isotropic condition, where the latter incorporates the different layers (Figure 2.1) which vary by five orders of magnitude using Equations 1, 2 and 3 for the horizontal and vertical layers respectively.

Table 2.4 Physical properties of the study area (from Fan et al., 1997)

Parameter	Unit	Value
Density of freshwater	$\text{kgm}^{-3}$	998.2
Density of saline water	$\text{kgm}^{-3}$	1149.17
Permeability	$\text{m}^2$	$1.0204 \times 10^{-13}$
Porosity	-----	0.35
Dispersivity (longitudinal & transverse respectively)	m	200 & 20 respectively
Depth of study Area	m	1300
Length of study area	m	13000
Aspect ratio	----	10
Length of recharge area	m	9425
Initial concentration	$\text{kgkg}^{-1}$	0.0003
Molecular diffusivity of halite	$\text{m}^2\text{s}^{-1}$	$1.0 \times 10^{-9}$
Coefficient of compressibility for the solid matrix	$\text{ms}^2\text{kg}^{-1}$	$1.0 \times 10^{-7}$
Coefficient of compressibility of water	$\text{ms}^2\text{kg}^{-1}$	$4.47 \times 10^{-10}$
Dynamic viscosity of water (at 20°C)	$\text{kgm}^{-1}\text{s}^{-1}$	0.0001

## CHAPTER 3

### DISCUSSIONS AND RESULTS

#### 3.1 Climatic Variability, Groundwater Flow and Solute Transport

Climate has been playing a vital role in controlling the movement of water within the groundwater system and has been relatively variable both spatially and temporally over a long period in and around the study area (Mason et al., 1998). The temporal variability of climate (mainly precipitation and temperature) for this study is obtained for the past 20 ka from the coupled catchment-lake model. The output of precipitation and temperature from the coupled catchment-lake model assisted to estimate the temporal distribution of groundwater recharge for the past 20 ka. Overall, Maxey-Eakin method with coupled catchment-lake model and aridity index helped estimate the temporal and spatial distribution of groundwater recharge since the LGM.



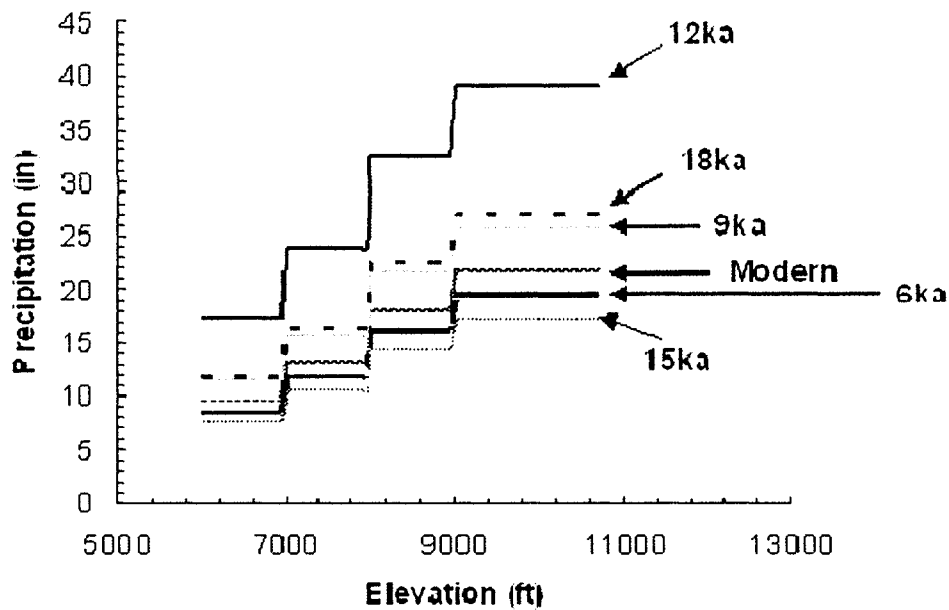


Figure 3.1 Precipitation distributions versus elevation for the past 20 ka based on Maxey-Eakin method and coupled catchment-lake model (Appendix 1).

Table 3.1 Groundwater recharge distribution with aridity index and factor to normalize the distribution of the index through time

Time (ka)	Temperature (°C)	precipitation (in)	recharge (m/yr)	Aridity Index	Factor
Modern	16.5	7.90	0.071	7.57	-----
6	17.7	7.11	0.060	6.52	0.86
9	17	9.48	0.083	8.92	1.18
12	12	14.22	0.170	16.42	2.17
15	14.7	6.32	0.063	6.50	0.86
18	11	9.88	0.128	11.94	1.58

It is imperative to consider temperature beside to precipitation in estimating groundwater recharge for the past periods, since there is a clear difference of temperature between present and past years (Table 5.1). According to Mifflin et al. (1979), pluvial

lake could have been maintained, if mean annual temperatures were approximately 5°F lower than today. Thus, the difference could influence the distribution of recharge. Otherwise, if only precipitation is considered as input to estimate recharge then the groundwater recharge will only mimic precipitation curve (Figure 3.2). The above table shows that an aridity index is assigned for each time period to average out the climatic variability and a factor is allocated for the past times based on the modern aridity index value. This factor helped normalize a groundwater recharge value for these periods by multiplying this factor to the present recharge value and these values seem to fit well for all simulation runs.

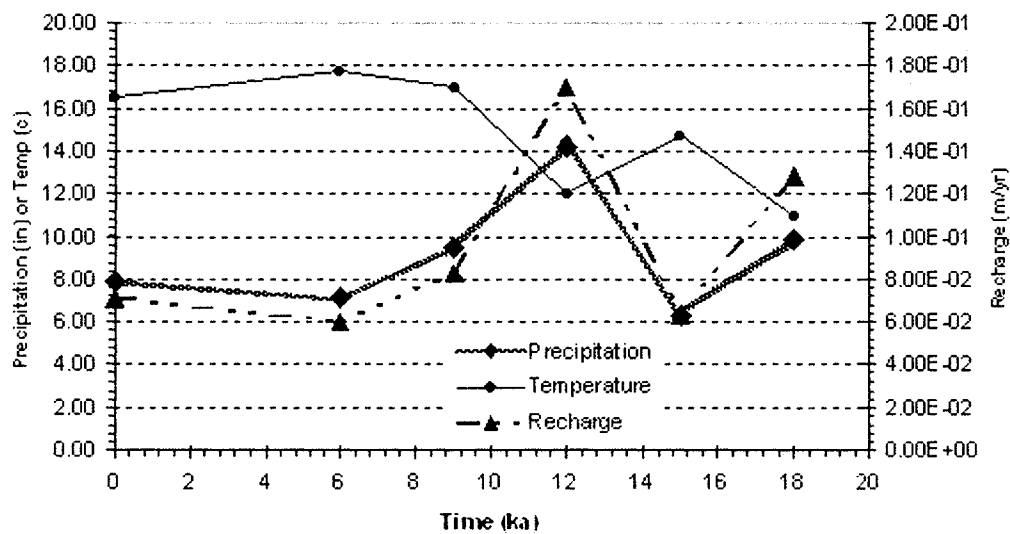


Figure 3.2 Distribution of precipitation, temperature and groundwater recharge using the Maxey-Eakin method with coupled catchment-lake model and aridity index.

The pluvial lake paleohydrology of the study area could have been maintained by mean annual temperatures lower than modern temperature, higher pluvial mean annual precipitation over modern precipitation and lesser pluvial mean annual evaporation than modern mean annual condition (Morrison, 1968). Further, estimates of the increase in mean annual precipitation from present mean values over the drainage area compared with those during the lake maximum ranged from 7-9 inches and a decrease of annual temperature, from 2.7-5 °F in the study area (Morrison, 1968). It is very important also to estimate groundwater recharge under variable climatic scenarios, because the solute concentration and its movement changes during dry and wet periods. This study shows that groundwater recharge variability directly influences the movement of salt wedge. Duffy and AL-Hassan (1988) explained that the salinity content of the closed lakes varies inversely with lake volume during climate fluctuations.

### 3.2 Simulations of Advective and Convective Flows under Homogeneous Condition

This study analyzes a unique relationship between both forced and free groundwater convections associated with variable climates and salinity gradients. A change in fluid density causes significant changes in the flow field, and this phenomenon is usually indicated as the density driven groundwater flow. The salinity gradients create free convection and initiate sinking of heavier water after a certain degree of instability is exceeded. Conductive factors for the free convection flow to take place are playa wetness, permeability of playa sediments, and regional climate and climate history (Fan et al., 1997). In this study, these factors are noticed to affect the flow system, where a wet playa, the case of wet period (12 ka) has obviously shallow water tables, which generate

the hydrologic connection with deep groundwater and consequently create a favorable environment for the free convection to take place. Further, the thick clay unit in Pilot Valley yields low permeability and subsequently yields slow solute transport into the subsurface and slows free convection by smoothing out the density front. Thirdly, the effect of climate on the free convection flow, where precipitation and evaporation seem to control the recharge, which are responsible for the playa wetness and formation of brines on the playa surface respectively. On the other hand, the forced convective (advective) flow which is a part of the natural groundwater system (Figure 1.3), the velocity of the convective motion has nothing to do with the fluid density. It is a natural occurring groundwater flow system, when precipitation percolates to the ground and moves from high elevation areas to low level areas due to the hydraulic gradient. Overall, the two types of flows are seen on the subsequent sections.

### 3.2.1 Simulation Results for Differing Time Series

The follow up resulting patterns offer an insight on how groundwater and density driven flows react to the effect of climatic variability which induce different groundwater recharges over a long period both spatially and temporally, and the salinity distribution on the playa.

Different distributions of groundwater recharge are prepared to correspond to rates of the different time periods (Figure 3.2) and a salinity range of 0.0003-0.2003 kgs/kg is applied over the time period. The circulation of freshwater and saline water and the position of the interface between the two are observed to respond to climatic and geologic variability.

#### 3.2.1.1 Initial Condition

The flow pattern on Figure 3.3 (b) shows the result of the initial condition where salinity is  $c=0.0003$  kgs/kg signifying the concentration of fresh lake water. At this point, the simulation is run with the homogeneous and steady state condition. The velocity fields describe that the advective flow is dominant, where the fresh water from the mountain discharges in the playa area. There is not enough salt accumulation that could allow free convection flow to happen. The groundwater flow patterns and fluxes reflect the condition of zero Rayleigh number. Furthermore, the higher recharge rate from the mountain side causes higher resistance to the salt front of the playa side and this causes a narrower mixing zone. The velocity vectors (Figure 3.3 (a)) show a maximum outlet at the hinge line, where they represent the velocity of the centroid of each element, approximated from the velocities at each node.

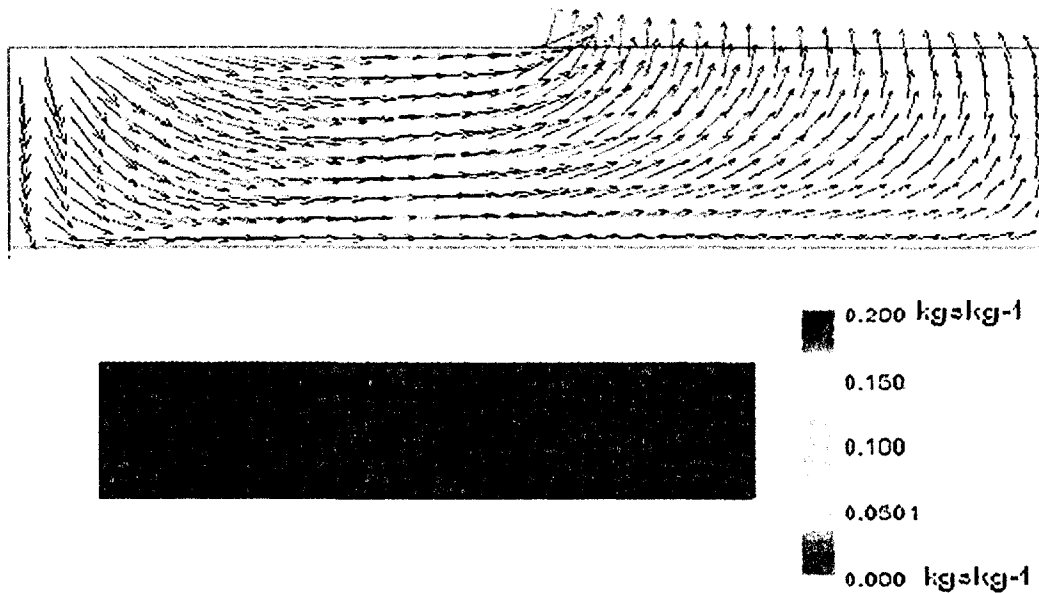


Figure 3.3 Steady state distributions (a) velocity fields and (b) playa concentrations under initial condition (legend shows kilogram of solute per kilogram of water ( $\text{kg/kg}^{-1}$ )).

### 3.2.1.2 Modern Condition

The groundwater recharge rate is present time recharge value and the salt concentration reaches to its maximum value of  $c=0.2003 \text{ (kg/kg}^{-1}\text{)}$  (Figure 3.4). Convective cells advance in the playa side and accelerate the salt transport at a relatively faster rate. At the same time, the salt wedge reaches the aquifer base and spreads towards the hinge line. Therefore, the spring is actually a mixture of fresh and salty water. Hence, the flow direction within the free convection cells is explained where the denser fluid on the low level area filled with evaporites creates a density gradient. The velocity fields of Figure 3.4 show that the movement of denser fluid to the surface and discharges on the playa as it starts mixing with the fresher water that comes from mountain side.

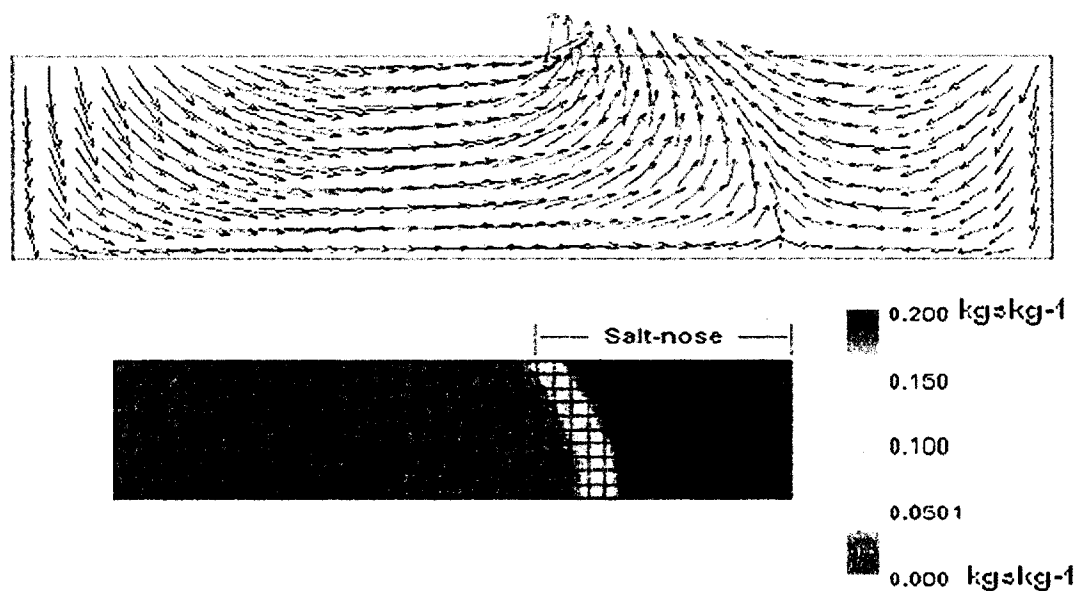


Figure 3.4 Steady state distributions (a) velocity fields and (b) playa concentrations and salt-extent under modern condition.

### 3.2.1.3 Simulation Result for 6 ka

This time period has less precipitation and higher temperature and these generate low groundwater recharge. The salt-nose and discharge area are wider as compared to present time. The groundwater recharge which plays a part on the Rayleigh equation has a significant effect on the outcome of this state. To demonstrate the utility of using the Rayleigh number as defined on Equation 7, the lower recharge causes more convective cells on the system and makes the salt-nose to penetrate relatively more towards the hinge line. Thus, the denser fluid causes relative stress to the incoming fresh water.

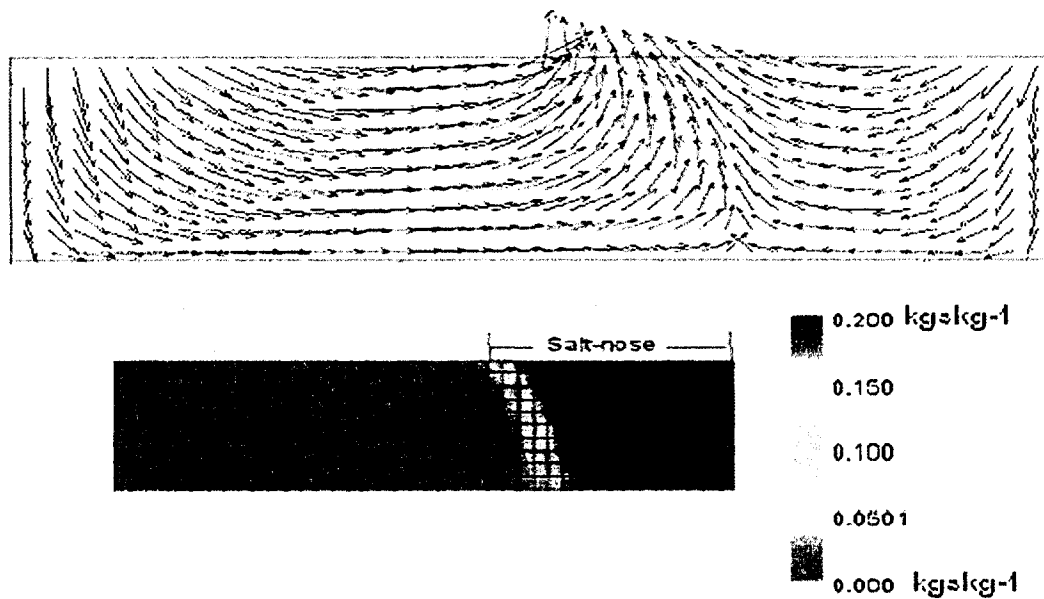


Figure 3.5 Steady state distributions (a) velocity fields and (b) playa concentrations and salt-nose extent for 6 ka.

#### 3.2.1.4 Simulation Result for 9 ka

The plume reaches the aquifer base and advances at relatively lower rate. The period has moderately higher groundwater recharge and covers greater discharge area than the preceding periods. The relative higher precipitation generates higher groundwater recharge and this seems to dominate and affect the groundwater flow and solute transport. The mixing zone between the fresh and saline water is pushed relatively to the playa side as compared to those in preceding periods. To illustrate using Rayleigh equation, the relative higher recharge velocity produces less Rayleigh number and this means less convective cells and narrow salt-nose in the flow system



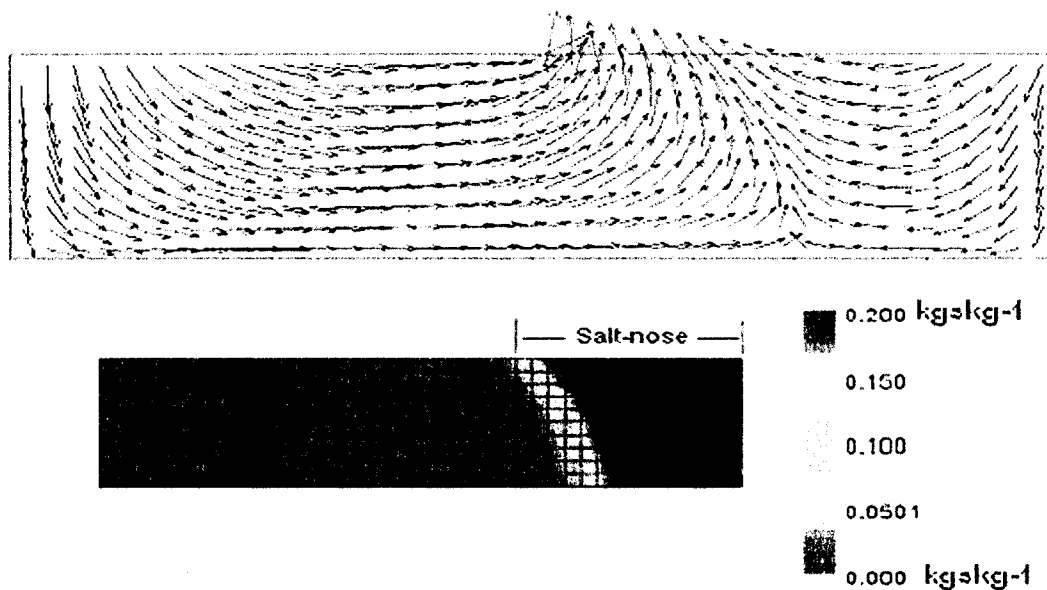


Figure 3.6 Steady state distributions (a) velocity fields and (b) playa concentrations and salt-nose extent for 9 ka.

### 3.2.1.5 Simulation Result for 12 ka

During the 12 ka time period, Lake Bonneville reached its maximum level and it was indicated by shorelines, deltas, bars and wave-cut inches in bedrock, as well as sedimentary deposits, and also four distinct strand lines have been recognized, which are pre-Bonneville strand at 5,100 feet altitude, the Bonneville strand at 5,135 feet, the Provo at 4,800 feet, and the Stanbury at 4,500 feet (Morrison, 1991).

During this period, the salt-nose moves far to the playa and covers smaller area; this is due to the concentration causes less resistance to the incoming groundwater recharge (Figure 3.7). At the same time, the plume does not reach the aquifer base, has a narrow mixing zone, and there is wider discharge area coverage. Furthermore, the higher

recharge velocity makes the salt wedge to be confined to a thin wedge and the freshwater to completely penetrate the margin of the basin.

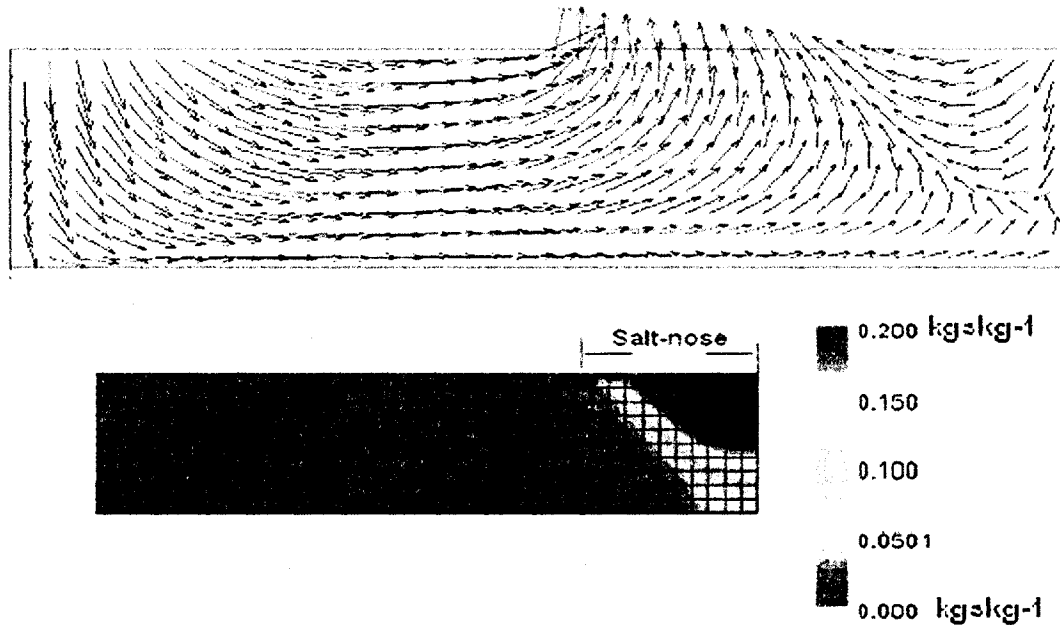


Figure 3.7 Steady state distributions (a) velocity fields and (b) playa concentrations and salt-nose extent for 12 ka.

#### 3.2.1.6 Simulation Result for 15 ka

This time period has relatively lower precipitation and temperature, as a result generates low groundwater recharge. After the 6 ka period, this time period produces low groundwater recharge in the past 20 ka. Hence, low recharge velocity means smaller Rayleigh number. Consequently, this causes relatively more convective cells and wider salt-nose in the flow system. Convective cells developed and efficiently distributed salt over the system, causing a complex spatial pattern of velocity and salinity throughout the simulation. The salt-nose extends far from the playa to the mountain side as compared to the present time.

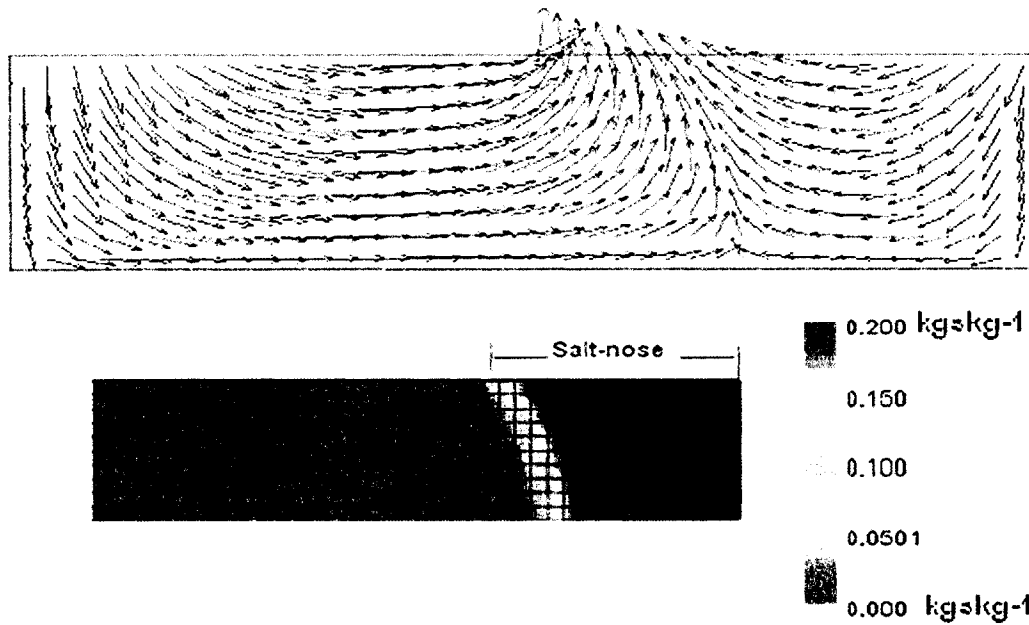


Figure 3.8 Steady state distributions (a) velocity fields and (b) playa concentrations and salt-nose extent for 15 ka.

### 3.2.1.7 Simulation Result for 18 ka

This time period is described by high precipitation and low temperature than present time. These scenarios generate higher groundwater recharge. Possessing high recharge velocity causes less convective cells and narrower salt-nose extent similar to the 12 ka time period. The discharge area has a greater coverage due to the high groundwater recharge caused mainly by high precipitation. The freshwater from the mountain side causes more stress to the denser fluid in the playa and seems to affect the spatial pattern of velocity fields and salinity.

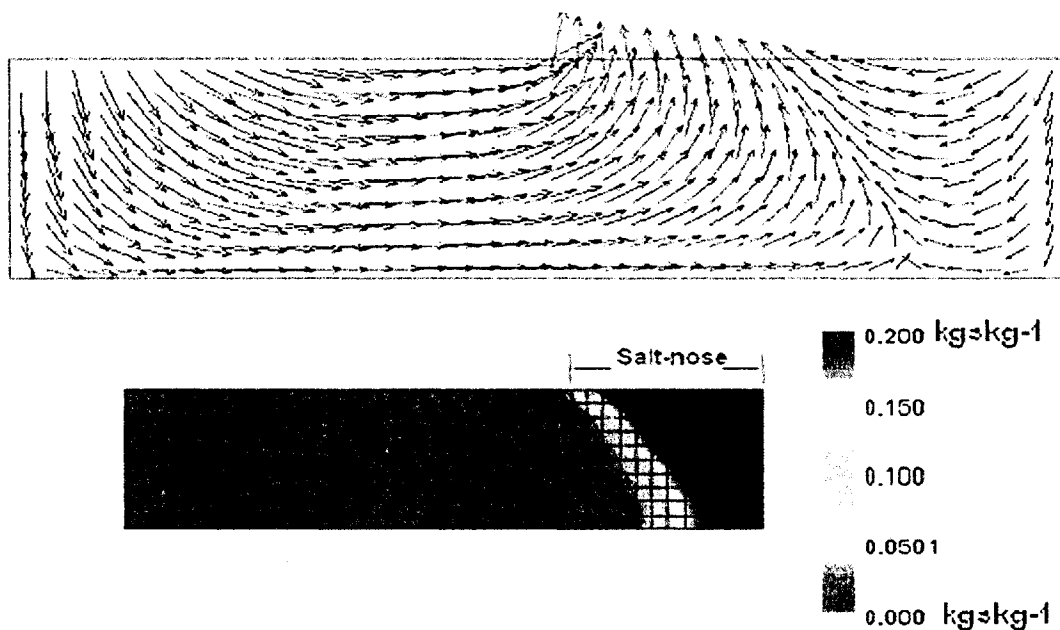


Figure 3.9 Steady state distributions (a) velocity fields and (b) playa concentrations and salt-nose extent for 18 ka.

Generally, the concentration distribution and the salt nose interface for different time series could be seen in Figure 3.10. Hence, the concentration distribution and salt-nose movement are seen to react to changes in groundwater recharge. Differing magnitude of groundwater recharge for different time periods appears to affect the pattern features of concentration and salt nose movement. Relatively narrow brine fingers penetrated into the underlying layers of the aquifer for high recharge periods (12 ka and 18 ka). Meanwhile, wider mixing zone or salt-nose is observed for periods with the lower groundwater recharge. These conditions could be explained by Rayleigh equation. Increase or decrease of recharge velocity could generate a decrease or increase of Rayleigh number respectively. For instance, the simulation run of the drier period (6 ka) illustrates the flow patterns and fluxes which evolve when Rayleigh number is high (low

recharge velocity). Further, the velocity field and salt concentration indicate that the salt-nose has migrated farther towards the hinge line. On the other hand, the simulation run of the wet period (12 ka) illustrates the flow patterns which develop under less Rayleigh number (high recharge velocity). This condition has relatively narrow salt-nose because the denser fluid creates less stress to the freshwater that comes from the mountain and pushed to the far end of the playa side.

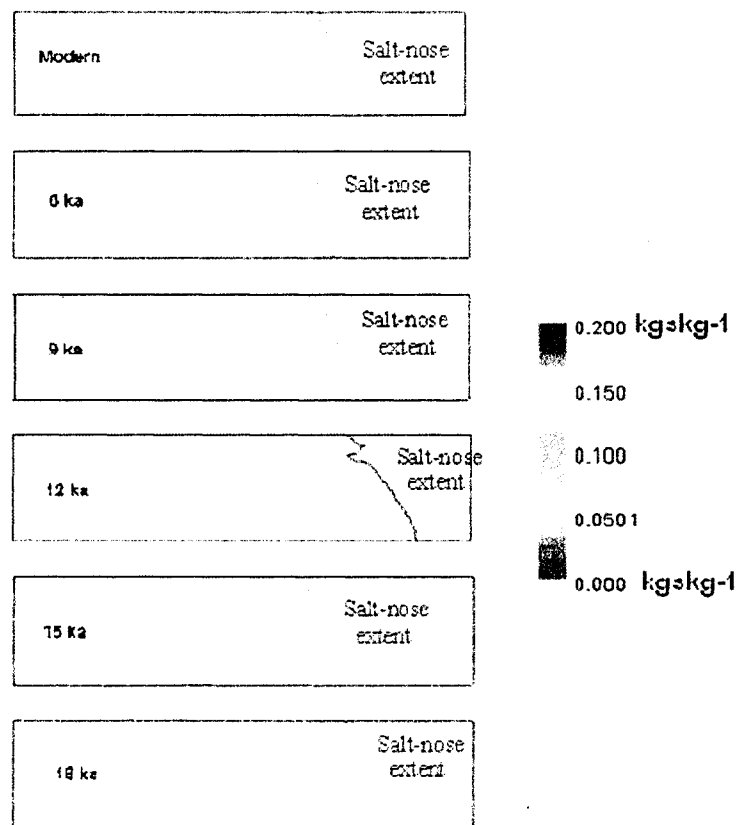


Figure 3.10 Extent of mixing zone or interface between fresh and saline water.

### 3.3 Geologic Variability

Geologic variability largely influences the heterogeneity of an aquifer (Weissmann et al., 1999). Geologic variability exists on many scales in complex aquifers, such as the study area where it is composed of fractured rocks, talus slopes, and alluvial fans (Figure 2.3). This variability should be taken into account in simulating the hydrology and geochemistry of the study area because it significantly influences the groundwater flow and solute transport. However, a detailed stratigraphic study is required to really understand the variability of an aquifer and this is beyond the scope of this research. For this study, the effect of geologic variability is assessed, by exaggerating or lessening permeability values by a magnitude for 12 ka and 6 ka periods. These time periods represent wet and dry conditions of the system respectively. By varying permeability value, the simulation patterns provide their relative impact on the flow system.

#### 3.3.1 Geologic Variability under Wet Period

Rayleigh number could offer evidence on how wet and dry periods respond with the increase or decrease of permeability value. Equation 7 describes any increase of buoyancy velocity (permeability) would increase Rayleigh number and consequentially increase the presence of convective cells. On the contrary, any increase of recharge velocity would decrease the presence of free convective flow and the reverse is true. These conditions are seen to respond on the follow up simulation result patterns.

Permeability value on the input data was amplified by one magnitude for the 12 ka (wet period) and this is observed to affect simulated groundwater flow and solute transport significantly. Further, there is a change on the thickness of the mixing zone

between the fresh and denser water. This observation is consistent throughout the time series.

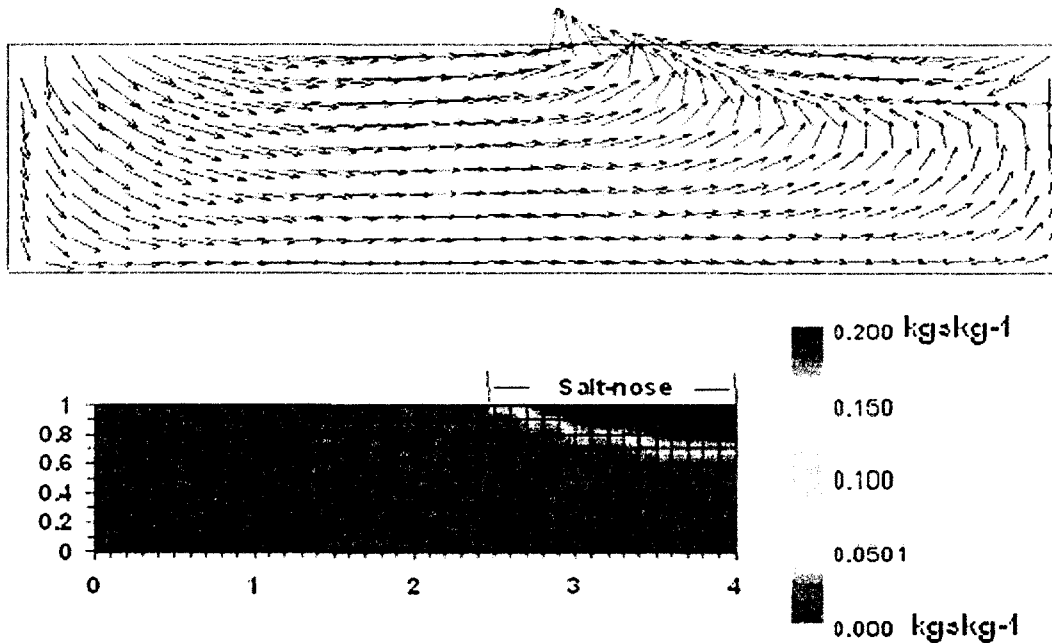


Figure 3.11 Effect of geologic variability (high permeability) and formation of free convective flow: (a) velocity fields and (b) playa concentrations and salt-nose extent for the wet period (12 ka).

The above response could be elaborated through Rayleigh equation by comparing to the homogeneous condition for the same time period (Figure 3.7). Though both simulation runs have the same recharge velocity, buoyancy velocity (permeability) is lower under the homogeneous condition (Figure 3.7). Therefore, for the same recharge, increasing one of the buoyancy velocity parameters in Rayleigh equation would obviously increase Rayleigh number and thus increases convective cells in the system (Figure 3.11). However, in the homogenous medium with relative less permeability for

the same period, the salt-nose was pushed comparatively farther to the playa side and has few convective cells (Figure 3.7).

Figure 3.12 describes the distribution of velocity fields and salt wedge under the wet period, and low permeability. In this simulation run, both permeability and groundwater recharge dictates the flow system. Low permeability initiates lower Rayleigh number, consequently prohibiting convective cells from developing. High groundwater recharge effectively limits the intrusion of saline water. Also, the brine water on the playa side of the simulation domain has no capacity to push the incoming stronger fresher water and as a result, the thinner salt wedge and wider discharge area is formed.

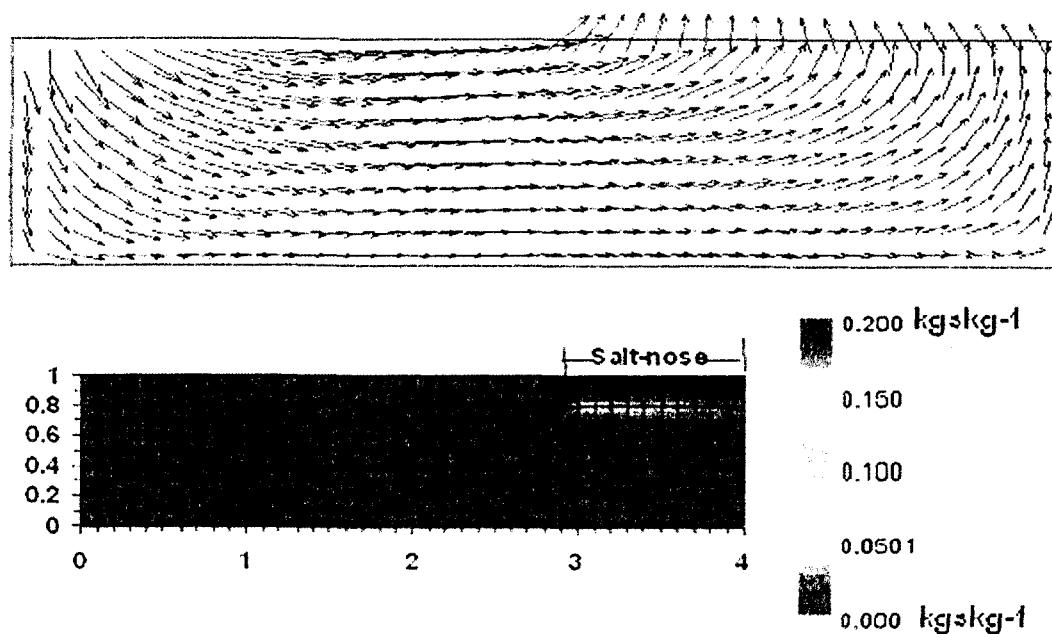


Figure 3.12 Effect of geologic variability (low permeability) and formation of free convective flow: (a) velocity fields and (b) playa concentrations and salt-nose extent for the wet period (12 ka).



The simulation shown in Figure 3.12 illustrates the flow patterns and fluxes which evolve when Rayleigh number is low or zero. Having higher recharge velocity and low buoyancy velocity in Rayleigh equation generates low or zero Rayleigh number and this means less or even no convective cells in the system (Figure 3.12). The recharge velocity of the freshwater from the mountain side associated with low permeability value, causes enough stress to limit the movement of the denser fluid in the playa side.

### 3.3.2 Geologic Variability under Dry Period

As described in previous sections, the 6 ka is characterized as dry period and has relatively low groundwater recharge. When low recharge velocity is associated with higher buoyancy velocity (permeability), it increases Rayleigh number. Also, High Rayleigh number means more convective cells in the system (Figure 3.13). Further, the salt-nose pushed towards of the hinge line and the freshwater zone relatively confined to a thin wedge. This situation represents a dry condition bounded by less precipitation which induced less groundwater recharge.

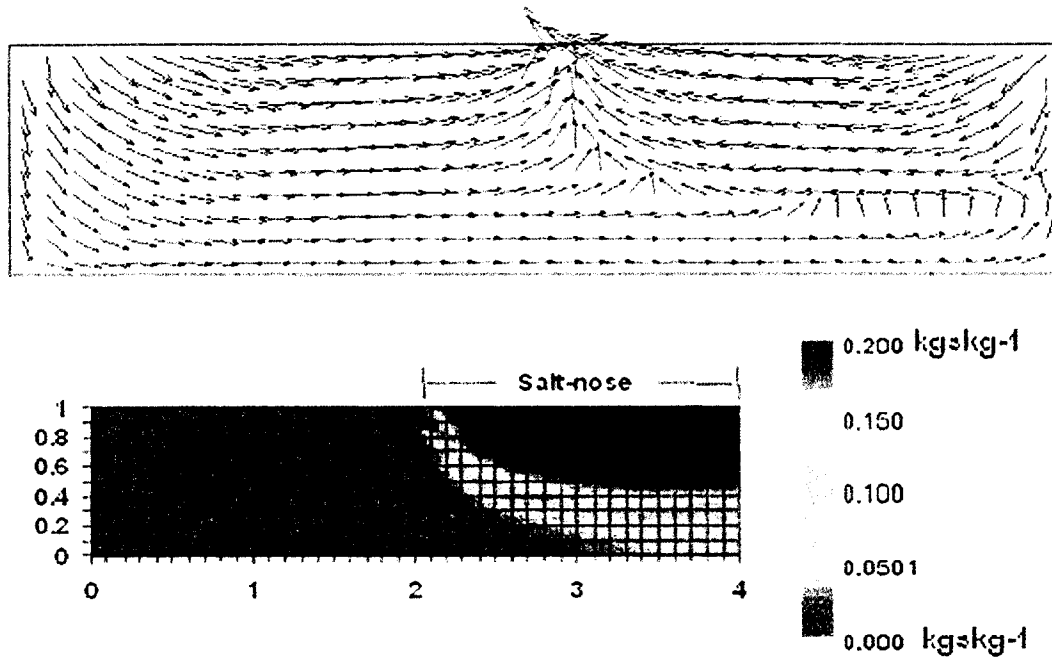


Figure 3.13 Effect of geologic variability (high permeability) and formation of free convective flow: (a) velocity fields and (b) playa concentrations and salt-nose extent for the dry period (6 ka).

The simulation shown in Figure 3.14 exemplifies the case when both recharge and buoyancy velocity are relatively low. The brine water in this simulation is noticed to move laterally along the top layer. Further, Rayleigh number is relatively low for this simulation than the same period with high buoyancy velocity (permeability). Low Rayleigh number causes less convective cells in the system. Thus, the salt wedge generates less stress to the incoming freshwater from the mountain side. Meanwhile, this simulation result shows relatively more convective cells on the far end of the playa than the simulation result of Figure 3.12 (wet period and low permeability), which have higher recharge and lower permeability and no convective cells. Hence, high recharge velocity

and low permeability minimize or even eliminate the effect of the denser fluid on the playa side.

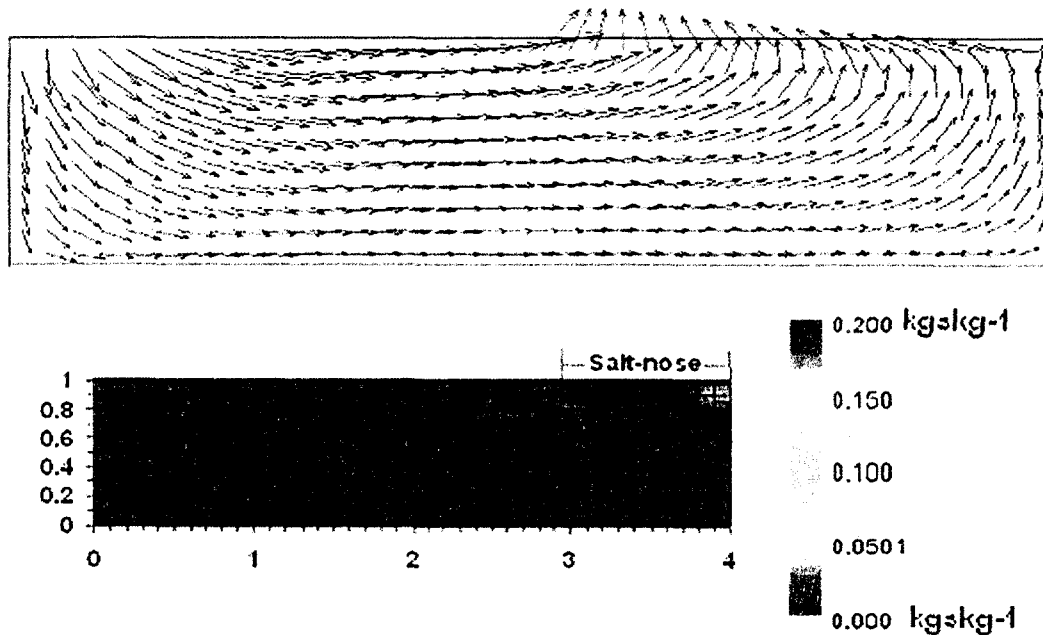


Figure 3.14 Effect of geologic variability (low permeability) and formation of free convective flow (a) velocity fields and (b) playa concentrations and salt-nose extent for the dry period (6 ka).

By large, the existence of geologic variability was seen to affect the development of free convection. It is obvious that applying a distinct permeability value for each stratum would give more apparent results. However, a permeability value for the top clay aquifer (Figure 2.1) would allow the convective flow to be developed only on the upper part of the aquifer and this is due to the clay sequence beneath the playa which causes the flow system to take longer to establish a detectable salt wedge and this geologic variability could change the pattern and complexity of free convection flow. That is why,

for this study the permeability values are taken to be effective constants, or basin wide averages to represent equivalent and homogeneous condition. This allows the simulation to isolate the effect of upper part of the aquifer (clay material).

## CHAPTER 4

### CONCLUSIONS AND RECOMMENDATIONS

The situations of groundwater flow and solute transport under density gradient have been examined in this study under different scenarios. These settings, which include climatic variability, the heterogeneity of aquifer and the scaling relationship of an area, were observed to affect the hydrology and geochemistry of the system. To setup the SUTRA model for various simulations, Maxey-Eakin method with coupled catchment-lake model and incomplete beta function for recharge distribution was used for the model simulations along with the pre- and post-processing of different data sets.

It is noticed that geologic variability affects groundwater flow and solute transport by changing the shape and spatial distribution of the salt nose and convective cells. This geologic variability is directly associated with Rayleigh number, which is a useful measure of the existence or absence of convective flows. It is revealed on the simulations that a higher Rayleigh number with a high buoyancy velocity (permeability) will cause the brine fluid to cover a wider area with saline water and creates more convective cells; on the contrary, low permeability generates lower Rayleigh number and would make the stronger fresher water that comes from the mountain to effectively limit the infringement of the brine and even eliminates convective cells.

The combination of saline concentration and the underlying groundwater results in a complex and dynamic hydrologic system that is susceptible to the climatic variability. The hydraulic head closely mimics topography and this induces a steady state flow between groundwater recharge and discharge areas over long time and this long time period accounts for the role of climatic variability on the groundwater flow. The variability tends to affect the hydrogeology of the system mainly through groundwater recharge, and the spatial orientation of the mixing zone between fresh and saline water.

Moreover, the impact seems to influence groundwater recharge temporally and spatially, where the former, during the period of high precipitation, the groundwater recharge was at its higher content and this was seen in simulations to affect the hydrology and geochemistry of the study area. In this case, the Rayleigh number is low and produced a narrow salt-nose with less convective cells, and the discharge area covers a larger portion and this leads to a lower salt concentration on the playa side. The reverse is true, in drier period (6 ka) with lower groundwater recharge produced a higher Rayleigh number, consequently shows more convective cells, wider brine area and smaller discharge area around the playa.

The physiographic nature of the area has a huge impact on the flow system, where high mountains and low level playa have a propensity to cause hydrologic implications in the spatial distribution of the groundwater recharge. Maxey-Eakin method, incomplete beta function and aridity index were applied to solve the scaling relationship. The incomplete beta function helped identify the length scale of the recharge and discharge area, by normalizing the overall height above sea level and the distance from the divide to the hinge line. Maxey-Eakin method, an empirical scheme provides relatively adequate

outcome of groundwater recharge, with the help of aridity index which is used to average and normalize the effect of climatic factors (precipitation and temperature).

In general, since the study area, a part of the Great Basin is susceptible to the climatic and geologic variability, a detailed study of climatic variability, geologic heterogeneity and scaling relationship would offer a better insight on how the system responds to each change. As described in the previous sections, climate changes the important boundary conditions: aquifer salinity and groundwater recharge. Understanding and output optimization of this variability of climate both temporally and spatially are indispensable for the clear realization of advective and convective flows. These two flows have a proclivity to affect the flow system and the upward or downward migration of dissolved halite. At the same time, the study area has a unique physiographic geology where it produces a scaling relationship between climate and topography; therefore further understanding of this scenario would offer valuable information because this relationship influences the hydrogeochemistry of the area. At last, geologic heterogeneity tends to affect the flow system and detailed examination of this variability by analyzing different strata along the aquifer would offer a better insight of the groundwater and density driven flow transport. For instance, the existence of clay material on the top layer of the surface could deter the free movement of the salt wedge and it will result in less convective cells to be developed along the aquifer.

There are several implications of this study in terms of water resources management and flood management perspectives. Since the area is known from its extreme hydrologic events, which causes tremendous damages to human lives, economic activity, and natural systems, the study will help minimize the damage and manage water

resources efficiently. In the past decade, there has been also increasing interests in using closed basins as repositories for low and high level toxic waste. It is known that radioactive, industrial, or saline wastes do not come into contact with the hydrologic flow system because of the permanent damage that might result. Therefore, additional field data and numerical experiments are essential in order to represent the physical system in a more realistic manner.



## APPENDIX 1

### RECHARGE DISTRIBUTION FOR ALL PERIODS

#### Groundwater Recharge Distribution for Modern Condition

Altitude (feet)	Precipitation (ft)	Precipitation (in)	Effective recharge	Recharge (ft/yr)	Recharge (m/yr)
10715	1.800	21.6	0.250	0.45	4.34932E-09
10615	1.800	21.6	0.250	0.45	4.34932E-09
10565	1.800	21.6	0.250	0.45	4.34932E-09
10515	1.800	21.6	0.250	0.45	4.34932E-09
10465	1.800	21.6	0.250	0.45	4.34932E-09
10415	1.800	21.6	0.250	0.45	4.34932E-09
10365	1.800	21.6	0.250	0.45	4.34932E-09
10315	1.800	21.6	0.250	0.45	4.34932E-09
10265	1.800	21.6	0.250	0.45	4.34932E-09
10215	1.800	21.6	0.250	0.45	4.34932E-09
10165	1.800	21.6	0.250	0.45	4.34932E-09
10115	1.800	21.6	0.250	0.45	4.34932E-09
10065	1.800	21.6	0.250	0.45	4.34932E-09
10015	1.800	21.6	0.250	0.45	4.34932E-09
9965	1.800	21.6	0.250	0.45	4.34932E-09
9915	1.800	21.6	0.250	0.45	4.34932E-09
9865	1.800	21.6	0.250	0.45	4.34932E-09
9815	1.800	21.6	0.250	0.45	4.34932E-09
9765	1.800	21.6	0.250	0.45	4.34932E-09
9715	1.800	21.6	0.250	0.45	4.34932E-09
9665	1.800	21.6	0.250	0.45	4.34932E-09
9615	1.800	21.6	0.250	0.45	4.34932E-09
9565	1.800	21.6	0.250	0.45	4.34932E-09
9515	1.800	21.6	0.250	0.45	4.34932E-09
9465	1.800	21.6	0.250	0.45	4.34932E-09
9415	1.800	21.6	0.250	0.45	4.34932E-09
9365	1.800	21.6	0.250	0.45	4.34932E-09
9315	1.800	21.6	0.250	0.45	4.34932E-09
9265	1.800	21.6	0.250	0.45	4.34932E-09
9215	1.800	21.6	0.250	0.45	4.34932E-09
9165	1.800	21.6	0.250	0.45	4.34932E-09
9115	1.800	21.6	0.250	0.45	4.34932E-09

9065	1.800	21.6	0.250	0.45	4.34932E-09
9015	1.800	21.6	0.250	0.45	4.34932E-09
8965	1.500	18	0.150	0.225	2.17466E-09
8915	1.500	18	0.150	0.225	2.17466E-09
8865	1.500	18	0.150	0.225	2.17466E-09
8815	1.500	18	0.150	0.225	2.17466E-09
8765	1.500	18	0.150	0.225	2.17466E-09
8715	1.500	18	0.150	0.225	2.17466E-09
8665	1.500	18	0.150	0.225	2.17466E-09
8615	1.500	18	0.150	0.225	2.17466E-09
8565	1.500	18	0.150	0.225	2.17466E-09
8515	1.500	18	0.150	0.225	2.17466E-09
8465	1.500	18	0.150	0.225	2.17466E-09
8415	1.500	18	0.150	0.225	2.17466E-09
8365	1.500	18	0.150	0.225	2.17466E-09
8315	1.500	18	0.150	0.225	2.17466E-09
8265	1.500	18	0.150	0.225	2.17466E-09
8215	1.500	18	0.150	0.225	2.17466E-09
8165	1.500	18	0.150	0.225	2.17466E-09
8115	1.500	18	0.150	0.225	2.17466E-09
8065	1.500	18	0.150	0.225	2.17466E-09
8015	1.500	18	0.150	0.225	2.17466E-09
7965	1.100	13.2	0.070	0.077	7.44216E-10
7915	1.100	13.2	0.070	0.077	7.44216E-10
7865	1.100	13.2	0.070	0.077	7.44216E-10
7815	1.100	13.2	0.070	0.077	7.44216E-10
7765	1.100	13.2	0.070	0.077	7.44216E-10
7715	1.100	13.2	0.070	0.077	7.44216E-10
7665	1.100	13.2	0.070	0.077	7.44216E-10
7615	1.100	13.2	0.070	0.077	7.44216E-10
7565	1.100	13.2	0.070	0.077	7.44216E-10
7515	1.100	13.2	0.070	0.077	7.44216E-10
7465	1.100	13.2	0.070	0.077	7.44216E-10
7415	1.100	13.2	0.070	0.077	7.44216E-10
7365	1.100	13.2	0.070	0.077	7.44216E-10
7315	1.100	13.2	0.070	0.077	7.44216E-10
7265	1.100	13.2	0.070	0.077	7.44216E-10
7215	1.100	13.2	0.070	0.077	7.44216E-10
7165	1.100	13.2	0.070	0.077	7.44216E-10
7115	1.100	13.2	0.070	0.077	7.44216E-10
7065	1.100	13.2	0.070	0.077	7.44216E-10
7015	1.100	13.2	0.070	0.077	7.44216E-10
6965	0.800	9.6	0.030	0.024	2.31963E-10
6915	0.800	9.6	0.030	0.024	2.31963E-10
6865	0.800	9.6	0.030	0.024	2.31963E-10
6815	0.800	9.6	0.030	0.024	2.31963E-10

6765	0.800	9.6	0.030	0.024	2.31963E-10
6715	0.800	9.6	0.030	0.024	2.31963E-10
6665	0.800	9.6	0.030	0.024	2.31963E-10
6615	0.800	9.6	0.030	0.024	2.31963E-10
6565	0.800	9.6	0.030	0.024	2.31963E-10
6515	0.800	9.6	0.030	0.024	2.31963E-10
6465	0.800	9.6	0.030	0.024	2.31963E-10
6415	0.800	9.6	0.030	0.024	2.31963E-10
6365	0.800	9.6	0.030	0.024	2.31963E-10
6315	0.800	9.6	0.030	0.024	2.31963E-10
6265	0.800	9.6	0.030	0.024	2.31963E-10
6215	0.800	9.6	0.030	0.024	2.31963E-10
6165	0.800	9.6	0.030	0.024	2.31963E-10
6115	0.800	9.6	0.030	0.024	2.31963E-10
6065	0.800	9.6	0.030	0.024	2.31963E-10
6015	0.800	9.6	0.030	0.024	2.31963E-10
5965	0.500	6	0.000	0	0
5915	0.500	6	0.000	0	0
5865	0.500	6	0.000	0	0

# Groundwater Recharge Distribution for 6 ka

Altitude (ft)	Precipitation (ft)	P-6ka	Precipitation (in)	Effective recharge	Recharge (ft/yr)	Recharge (m/yr)
10715	1.800	1.620	19.44	0.150	0.243	2.34863E-09
10615	1.800	1.620	19.44	0.150	0.243	2.34863E-09
10565	1.800	1.620	19.44	0.150	0.243	2.34863E-09
10515	1.800	1.620	19.44	0.150	0.243	2.34863E-09
10465	1.800	1.620	19.44	0.150	0.243	2.34863E-09
10415	1.800	1.620	19.44	0.150	0.243	2.34863E-09
10365	1.800	1.620	19.44	0.150	0.243	2.34863E-09
10315	1.800	1.620	19.44	0.150	0.243	2.34863E-09
10265	1.800	1.620	19.44	0.150	0.243	2.34863E-09
10215	1.800	1.620	19.44	0.150	0.243	2.34863E-09
10165	1.800	1.620	19.44	0.150	0.243	2.34863E-09
10115	1.800	1.620	19.44	0.150	0.243	2.34863E-09
10065	1.800	1.620	19.44	0.150	0.243	2.34863E-09
10015	1.800	1.620	19.44	0.150	0.243	2.34863E-09
9965	1.800	1.620	19.44	0.150	0.243	2.34863E-09
9915	1.800	1.620	19.44	0.150	0.243	2.34863E-09
9865	1.800	1.620	19.44	0.150	0.243	2.34863E-09
9815	1.800	1.620	19.44	0.150	0.243	2.34863E-09
9765	1.800	1.620	19.44	0.150	0.243	2.34863E-09
9715	1.800	1.620	19.44	0.150	0.243	2.34863E-09
9665	1.800	1.620	19.44	0.150	0.243	2.34863E-09
9615	1.800	1.620	19.44	0.150	0.243	2.34863E-09
9565	1.800	1.620	19.44	0.150	0.243	2.34863E-09
9515	1.800	1.620	19.44	0.150	0.243	2.34863E-09
9465	1.800	1.620	19.44	0.150	0.243	2.34863E-09
9415	1.800	1.620	19.44	0.150	0.243	2.34863E-09
9365	1.800	1.620	19.44	0.150	0.243	2.34863E-09
9315	1.800	1.620	19.44	0.150	0.243	2.34863E-09
9265	1.800	1.620	19.44	0.150	0.243	2.34863E-09
9215	1.800	1.620	19.44	0.150	0.243	2.34863E-09
9165	1.800	1.620	19.44	0.150	0.243	2.34863E-09
9115	1.800	1.620	19.44	0.150	0.243	2.34863E-09
9065	1.800	1.620	19.44	0.150	0.243	2.34863E-09
9015	1.800	1.620	19.44	0.150	0.243	2.34863E-09
8965	1.500	1.350	16.2	0.150	0.2025	1.95719E-09
8915	1.500	1.350	16.2	0.150	0.2025	1.95719E-09
8865	1.500	1.350	16.2	0.150	0.2025	1.95719E-09
8815	1.500	1.350	16.2	0.150	0.2025	1.95719E-09
8765	1.500	1.350	16.2	0.150	0.2025	1.95719E-09
8715	1.500	1.350	16.2	0.150	0.2025	1.95719E-09
8665	1.500	1.350	16.2	0.150	0.2025	1.95719E-09
8615	1.500	1.350	16.2	0.150	0.2025	1.95719E-09

8565	1.500	1.350	16.2	0.150	0.2025	1.95719E-09
8515	1.500	1.350	16.2	0.150	0.2025	1.95719E-09
8465	1.500	1.350	16.2	0.150	0.2025	1.95719E-09
8415	1.500	1.350	16.2	0.150	0.2025	1.95719E-09
8365	1.500	1.350	16.2	0.150	0.2025	1.95719E-09
8315	1.500	1.350	16.2	0.150	0.2025	1.95719E-09
8265	1.500	1.350	16.2	0.150	0.2025	1.95719E-09
8215	1.500	1.350	16.2	0.150	0.2025	1.95719E-09
8165	1.500	1.350	16.2	0.150	0.2025	1.95719E-09
8115	1.500	1.350	16.2	0.150	0.2025	1.95719E-09
8065	1.500	1.350	16.2	0.150	0.2025	1.95719E-09
8015	1.500	1.350	16.2	0.150	0.2025	1.95719E-09
7965	1.100	0.990	11.88	0.030	0.0297	2.87055E-10
7915	1.100	0.990	11.88	0.030	0.0297	2.87055E-10
7865	1.100	0.990	11.88	0.030	0.0297	2.87055E-10
7815	1.100	0.990	11.88	0.030	0.0297	2.87055E-10
7765	1.100	0.990	11.88	0.030	0.0297	2.87055E-10
7715	1.100	0.990	11.88	0.030	0.0297	2.87055E-10
7665	1.100	0.990	11.88	0.030	0.0297	2.87055E-10
7615	1.100	0.990	11.88	0.030	0.0297	2.87055E-10
7565	1.100	0.990	11.88	0.030	0.0297	2.87055E-10
7515	1.100	0.990	11.88	0.030	0.0297	2.87055E-10
7465	1.100	0.990	11.88	0.030	0.0297	2.87055E-10
7415	1.100	0.990	11.88	0.030	0.0297	2.87055E-10
7365	1.100	0.990	11.88	0.030	0.0297	2.87055E-10
7315	1.100	0.990	11.88	0.030	0.0297	2.87055E-10
7265	1.100	0.990	11.88	0.030	0.0297	2.87055E-10
7215	1.100	0.990	11.88	0.030	0.0297	2.87055E-10
7165	1.100	0.990	11.88	0.030	0.0297	2.87055E-10
7115	1.100	0.990	11.88	0.030	0.0297	2.87055E-10
7065	1.100	0.990	11.88	0.030	0.0297	2.87055E-10
7015	1.100	0.990	11.88	0.030	0.0297	2.87055E-10
6965	0.800	0.720	8.64	0.030	0.0216	2.08767E-10
6915	0.800	0.720	8.64	0.030	0.0216	2.08767E-10
6865	0.800	0.720	8.64	0.030	0.0216	2.08767E-10
6815	0.800	0.720	8.64	0.030	0.0216	2.08767E-10
6765	0.800	0.720	8.64	0.030	0.0216	2.08767E-10
6715	0.800	0.720	8.64	0.030	0.0216	2.08767E-10
6665	0.800	0.720	8.64	0.030	0.0216	2.08767E-10
6615	0.800	0.720	8.64	0.030	0.0216	2.08767E-10
6565	0.800	0.720	8.64	0.030	0.0216	2.08767E-10
6515	0.800	0.720	8.64	0.030	0.0216	2.08767E-10
6465	0.800	0.720	8.64	0.030	0.0216	2.08767E-10
6415	0.800	0.720	8.64	0.030	0.0216	2.08767E-10
6365	0.800	0.720	8.64	0.030	0.0216	2.08767E-10
6315	0.800	0.720	8.64	0.030	0.0216	2.08767E-10

6265	0.800	0.720	8.64	0.030	0.0216	2.08767E-10
6215	0.800	0.720	8.64	0.030	0.0216	2.08767E-10
6165	0.800	0.720	8.64	0.030	0.0216	2.08767E-10
6115	0.800	0.720	8.64	0.030	0.0216	2.08767E-10
6065	0.800	0.720	8.64	0.030	0.0216	2.08767E-10
6015	0.800	0.720	8.64	0.030	0.0216	2.08767E-10
5965	0.500	0.450	5.4	0.000	0	0
5915	0.500	0.450	5.4	0.000	0	0
5865	0.500	0.450	5.4	0.000	0	0

Groundwater Recharge Distribution for 9 ka						
Altitude (ft)	Precipitation (ft)	P-9ka	Precipitation (in)	Effective recharge	Recharge (ft/yr)	Recharge (m/yr)
10715	1.800	2.160	25.92	0.250	0.54	5.21918E-09
10615	1.800	2.160	25.92	0.250	0.54	5.21918E-09
10565	1.800	2.160	25.92	0.250	0.54	5.21918E-09
10515	1.800	2.160	25.92	0.250	0.54	5.21918E-09
10465	1.800	2.160	25.92	0.250	0.54	5.21918E-09
10415	1.800	2.160	25.92	0.250	0.54	5.21918E-09
10365	1.800	2.160	25.92	0.250	0.54	5.21918E-09
10315	1.800	2.160	25.92	0.250	0.54	5.21918E-09
10265	1.800	2.160	25.92	0.250	0.54	5.21918E-09
10215	1.800	2.160	25.92	0.250	0.54	5.21918E-09
10165	1.800	2.160	25.92	0.250	0.54	5.21918E-09
10115	1.800	2.160	25.92	0.250	0.54	5.21918E-09
10065	1.800	2.160	25.92	0.250	0.54	5.21918E-09
10015	1.800	2.160	25.92	0.250	0.54	5.21918E-09
9965	1.800	2.160	25.92	0.250	0.54	5.21918E-09
9915	1.800	2.160	25.92	0.250	0.54	5.21918E-09
9865	1.800	2.160	25.92	0.250	0.54	5.21918E-09
9815	1.800	2.160	25.92	0.250	0.54	5.21918E-09
9765	1.800	2.160	25.92	0.250	0.54	5.21918E-09
9715	1.800	2.160	25.92	0.250	0.54	5.21918E-09
9665	1.800	2.160	25.92	0.250	0.54	5.21918E-09
9615	1.800	2.160	25.92	0.250	0.54	5.21918E-09
9565	1.800	2.160	25.92	0.250	0.54	5.21918E-09
9515	1.800	2.160	25.92	0.250	0.54	5.21918E-09
9465	1.800	2.160	25.92	0.250	0.54	5.21918E-09
9415	1.800	2.160	25.92	0.250	0.54	5.21918E-09
9365	1.800	2.160	25.92	0.250	0.54	5.21918E-09
9315	1.800	2.160	25.92	0.250	0.54	5.21918E-09
9265	1.800	2.160	25.92	0.250	0.54	5.21918E-09
9215	1.800	2.160	25.92	0.250	0.54	5.21918E-09
9165	1.800	2.160	25.92	0.250	0.54	5.21918E-09
9115	1.800	2.160	25.92	0.250	0.54	5.21918E-09
9065	1.800	2.160	25.92	0.250	0.54	5.21918E-09
9015	1.800	2.160	25.92	0.250	0.54	5.21918E-09
8965	1.500	1.800	21.6	0.250	0.45	4.34932E-09
8915	1.500	1.800	21.6	0.250	0.45	4.34932E-09
8865	1.500	1.800	21.6	0.250	0.45	4.34932E-09

8815	1.500	1.800	21.6	0.250	0.45	4.34932E-09
8765	1.500	1.800	21.6	0.250	0.45	4.34932E-09
8715	1.500	1.800	21.6	0.250	0.45	4.34932E-09
8665	1.500	1.800	21.6	0.250	0.45	4.34932E-09
8615	1.500	1.800	21.6	0.250	0.45	4.34932E-09
8565	1.500	1.800	21.6	0.250	0.45	4.34932E-09
8515	1.500	1.800	21.6	0.250	0.45	4.34932E-09
8465	1.500	1.800	21.6	0.250	0.45	4.34932E-09
8415	1.500	1.800	21.6	0.250	0.45	4.34932E-09
8365	1.500	1.800	21.6	0.250	0.45	4.34932E-09
8315	1.500	1.800	21.6	0.250	0.45	4.34932E-09
8265	1.500	1.800	21.6	0.250	0.45	4.34932E-09
8215	1.500	1.800	21.6	0.250	0.45	4.34932E-09
8165	1.500	1.800	21.6	0.250	0.45	4.34932E-09
8115	1.500	1.800	21.6	0.250	0.45	4.34932E-09
8065	1.500	1.800	21.6	0.250	0.45	4.34932E-09
8015	1.500	1.800	21.6	0.250	0.45	4.34932E-09
7965	1.100	1.320	15.84	0.150	0.198	1.91370E-09
7915	1.100	1.320	15.84	0.150	0.198	1.91370E-09
7865	1.100	1.320	15.84	0.150	0.198	1.91370E-09
7815	1.100	1.320	15.84	0.150	0.198	1.91370E-09
7765	1.100	1.320	15.84	0.150	0.198	1.91370E-09
7715	1.100	1.320	15.84	0.150	0.198	1.91370E-09
7665	1.100	1.320	15.84	0.150	0.198	1.91370E-09
7615	1.100	1.320	15.84	0.150	0.198	1.91370E-09
7565	1.100	1.320	15.84	0.150	0.198	1.91370E-09
7515	1.100	1.320	15.84	0.150	0.198	1.91370E-09
7465	1.100	1.320	15.84	0.150	0.198	1.91370E-09
7415	1.100	1.320	15.84	0.150	0.198	1.91370E-09
7365	1.100	1.320	15.84	0.150	0.198	1.91370E-09
7315	1.100	1.320	15.84	0.150	0.198	1.91370E-09
7265	1.100	1.320	15.84	0.150	0.198	1.91370E-09
7215	1.100	1.320	15.84	0.150	0.198	1.91370E-09
7165	1.100	1.320	15.84	0.150	0.198	1.91370E-09
7115	1.100	1.320	15.84	0.150	0.198	1.91370E-09
7065	1.100	1.320	15.84	0.150	0.198	1.91370E-09
7015	1.100	1.320	15.84	0.150	0.198	1.91370E-09
6965	0.800	0.960	11.52	0.030	0.0288	2.78356E-10
6915	0.800	0.960	11.52	0.030	0.0288	2.78356E-10
6865	0.800	0.960	11.52	0.030	0.0288	2.78356E-10
6815	0.800	0.960	11.52	0.030	0.0288	2.78356E-10
6765	0.800	0.960	11.52	0.030	0.0288	2.78356E-10
6715	0.800	0.960	11.52	0.030	0.0288	2.78356E-10
6665	0.800	0.960	11.52	0.030	0.0288	2.78356E-10
6615	0.800	0.960	11.52	0.030	0.0288	2.78356E-10
6565	0.800	0.960	11.52	0.030	0.0288	2.78356E-10



6515	0.800	0.960	11.52	0.030	0.0288	2.78356E-10
6465	0.800	0.960	11.52	0.030	0.0288	2.78356E-10
6415	0.800	0.960	11.52	0.030	0.0288	2.78356E-10
6365	0.800	0.960	11.52	0.030	0.0288	2.78356E-10
6315	0.800	0.960	11.52	0.030	0.0288	2.78356E-10
6265	0.800	0.960	11.52	0.030	0.0288	2.78356E-10
6215	0.800	0.960	11.52	0.030	0.0288	2.78356E-10
6165	0.800	0.960	11.52	0.030	0.0288	2.78356E-10
6115	0.800	0.960	11.52	0.030	0.0288	2.78356E-10
6065	0.800	0.960	11.52	0.030	0.0288	2.78356E-10
6015	0.800	0.960	11.52	0.030	0.0288	2.78356E-10
5965	0.500	0.600	7.2	0.000	0	0
5915	0.500	0.600	7.2	0.000	0	0
5865	0.500	0.600	7.2	0.000	0	0

Groundwater Recharge Distribution for 12 ka

Altitude (ft)	Precipitation (ft)	P-12ka	Precipitation (in)	Effective recharge	Recharge (ft/yr)	Recharge (m/yr)
10715	1.800	3.240	38.88	0.250	0.81	7.82877E-09
10615	1.800	3.240	38.88	0.250	0.81	7.82877E-09
10565	1.800	3.240	38.88	0.250	0.81	7.82877E-09
10515	1.800	3.240	38.88	0.250	0.81	7.82877E-09
10465	1.800	3.240	38.88	0.250	0.81	7.82877E-09
10415	1.800	3.240	38.88	0.250	0.81	7.82877E-09
10365	1.800	3.240	38.88	0.250	0.81	7.82877E-09
10315	1.800	3.240	38.88	0.250	0.81	7.82877E-09
10265	1.800	3.240	38.88	0.250	0.81	7.82877E-09
10215	1.800	3.240	38.88	0.250	0.81	7.82877E-09
10165	1.800	3.240	38.88	0.250	0.81	7.82877E-09
10115	1.800	3.240	38.88	0.250	0.81	7.82877E-09
10065	1.800	3.240	38.88	0.250	0.81	7.82877E-09
10015	1.800	3.240	38.88	0.250	0.81	7.82877E-09
9965	1.800	3.240	38.88	0.250	0.81	7.82877E-09
9915	1.800	3.240	38.88	0.250	0.81	7.82877E-09
9865	1.800	3.240	38.88	0.250	0.81	7.82877E-09
9815	1.800	3.240	38.88	0.250	0.81	7.82877E-09
9765	1.800	3.240	38.88	0.250	0.81	7.82877E-09
9715	1.800	3.240	38.88	0.250	0.81	7.82877E-09
9665	1.800	3.240	38.88	0.250	0.81	7.82877E-09
9615	1.800	3.240	38.88	0.250	0.81	7.82877E-09
9565	1.800	3.240	38.88	0.250	0.81	7.82877E-09
9515	1.800	3.240	38.88	0.250	0.81	7.82877E-09
9465	1.800	3.240	38.88	0.250	0.81	7.82877E-09
9415	1.800	3.240	38.88	0.250	0.81	7.82877E-09
9365	1.800	3.240	38.88	0.250	0.81	7.82877E-09
9315	1.800	3.240	38.88	0.250	0.81	7.82877E-09
9265	1.800	3.240	38.88	0.250	0.81	7.82877E-09
9215	1.800	3.240	38.88	0.250	0.81	7.82877E-09
9165	1.800	3.240	38.88	0.250	0.81	7.82877E-09
9115	1.800	3.240	38.88	0.250	0.81	7.82877E-09
9065	1.800	3.240	38.88	0.250	0.81	7.82877E-09
9015	1.800	3.240	38.88	0.250	0.81	7.82877E-09
8965	1.500	2.700	32.4	0.250	0.675	6.52397E-09
8915	1.500	2.700	32.4	0.250	0.675	6.52397E-09
8865	1.500	2.700	32.4	0.250	0.675	6.52397E-09
8815	1.500	2.700	32.4	0.250	0.675	6.52397E-09

8765	1.500	2.700	32.4	0.250	0.675	6.52397E-09
8715	1.500	2.700	32.4	0.250	0.675	6.52397E-09
8665	1.500	2.700	32.4	0.250	0.675	6.52397E-09
8615	1.500	2.700	32.4	0.250	0.675	6.52397E-09
8565	1.500	2.700	32.4	0.250	0.675	6.52397E-09
8515	1.500	2.700	32.4	0.250	0.675	6.52397E-09
8465	1.500	2.700	32.4	0.250	0.675	6.52397E-09
8415	1.500	2.700	32.4	0.250	0.675	6.52397E-09
8365	1.500	2.700	32.4	0.250	0.675	6.52397E-09
8315	1.500	2.700	32.4	0.250	0.675	6.52397E-09
8265	1.500	2.700	32.4	0.250	0.675	6.52397E-09
8215	1.500	2.700	32.4	0.250	0.675	6.52397E-09
8165	1.500	2.700	32.4	0.250	0.675	6.52397E-09
8115	1.500	2.700	32.4	0.250	0.675	6.52397E-09
8065	1.500	2.700	32.4	0.250	0.675	6.52397E-09
8015	1.500	2.700	32.4	0.250	0.675	6.52397E-09
7965	1.100	1.980	23.76	0.250	0.495	4.78425E-09
7915	1.100	1.980	23.76	0.250	0.495	4.78425E-09
7865	1.100	1.980	23.76	0.250	0.495	4.78425E-09
7815	1.100	1.980	23.76	0.250	0.495	4.78425E-09
7765	1.100	1.980	23.76	0.250	0.495	4.78425E-09
7715	1.100	1.980	23.76	0.250	0.495	4.78425E-09
7665	1.100	1.980	23.76	0.250	0.495	4.78425E-09
7615	1.100	1.980	23.76	0.250	0.495	4.78425E-09
7565	1.100	1.980	23.76	0.250	0.495	4.78425E-09
7515	1.100	1.980	23.76	0.250	0.495	4.78425E-09
7465	1.100	1.980	23.76	0.250	0.495	4.78425E-09
7415	1.100	1.980	23.76	0.250	0.495	4.78425E-09
7365	1.100	1.980	23.76	0.250	0.495	4.78425E-09
7315	1.100	1.980	23.76	0.250	0.495	4.78425E-09
7265	1.100	1.980	23.76	0.250	0.495	4.78425E-09
7215	1.100	1.980	23.76	0.250	0.495	4.78425E-09
7165	1.100	1.980	23.76	0.250	0.495	4.78425E-09
7115	1.100	1.980	23.76	0.250	0.495	4.78425E-09
7065	1.100	1.980	23.76	0.250	0.495	4.78425E-09
7015	1.100	1.980	23.76	0.250	0.495	4.78425E-09
6965	0.800	1.440	17.28	0.150	0.216	2.08767E-09
6915	0.800	1.440	17.28	0.150	0.216	2.08767E-09
6865	0.800	1.440	17.28	0.150	0.216	2.08767E-09
6815	0.800	1.440	17.28	0.150	0.216	2.08767E-09
6765	0.800	1.440	17.28	0.150	0.216	2.08767E-09
6715	0.800	1.440	17.28	0.150	0.216	2.08767E-09

6665	0.800	1.440	17.28	0.150	0.216	2.08767E-09
6615	0.800	1.440	17.28	0.150	0.216	2.08767E-09
6565	0.800	1.440	17.28	0.150	0.216	2.08767E-09
6515	0.800	1.440	17.28	0.150	0.216	2.08767E-09
6465	0.800	1.440	17.28	0.150	0.216	2.08767E-09
6415	0.800	1.440	17.28	0.150	0.216	2.08767E-09
6365	0.800	1.440	17.28	0.150	0.216	2.08767E-09
6315	0.800	1.440	17.28	0.150	0.216	2.08767E-09
6265	0.800	1.440	17.28	0.150	0.216	2.08767E-09
6215	0.800	1.440	17.28	0.150	0.216	2.08767E-09
6165	0.800	1.440	17.28	0.150	0.216	2.08767E-09
6115	0.800	1.440	17.28	0.150	0.216	2.08767E-09
6065	0.800	1.440	17.28	0.150	0.216	2.08767E-09
6015	0.800	1.440	17.28	0.150	0.216	2.08767E-09
5965	0.500	0.900	10.8	0.030	0.027	2.60959E-10
5915	0.500	0.900	10.8	0.030	0.027	2.60959E-10
5865	0.500	0.900	10.8	0.030	0.027	2.60959E-10
5815	0.500	0.900	10.8	0.030	0.027	2.60959E-10
5765	0.500	0.900	10.8	0.030	0.027	2.60959E-10
5715	0.500	0.900	10.8	0.030	0.027	2.60959E-10
5665	0.500	0.900	10.8	0.030	0.027	2.60959E-10
5615	0.500	0.900	10.8	0.030	0.027	2.60959E-10
5565	0.500	0.900	10.8	0.030	0.027	2.60959E-10
5515	0.500	0.900	10.8	0.030	0.027	2.60959E-10
5465	0.500	0.900	10.8	0.030	0.027	2.60959E-10
5415	0.500	0.900	10.8	0.030	0.027	2.60959E-10
5365	0.500	0.900	10.8	0.030	0.027	2.60959E-10
5315	0.500	0.900	10.8	0.030	0.027	2.60959E-10
5265	0.500	0.900	10.8	0.030	0.027	2.60959E-10
5215	0.500	0.900	10.8	0.030	0.027	2.60959E-10
5165	0.500	0.900	10.8	0.030	0.027	2.60959E-10
5115	0.500	0.900	10.8	0.030	0.027	2.60959E-10
5065	0.500	0.900	10.8	0.030	0.027	2.60959E-10
5015	0.500	0.900	10.8	0.030	0.027	2.60959E-10
4965	0.500	0.900	10.8	0.030	0.027	2.60959E-10
4915	0.500	0.900	10.8	0.030	0.027	2.60959E-10
4865	0.500	0.900	10.8	0.030	0.027	2.60959E-10
4815	0.500	0.900	10.8	0.030	0.027	2.60959E-10
4765	0.500	0.900	10.8	0.030	0.027	2.60959E-10
4715	0.500	0.900	10.8	0.030	0.027	2.60959E-10
4665	0.500	0.900	10.8	0.030	0.027	2.60959E-10
4615	0.500	0.900	10.8	0.030	0.027	2.60959E-10

4565	0.500	0.900	10.8	0.030	0.027	2.60959E-10
4515	0.500	0.900	10.8	0.030	0.027	2.60959E-10
4465	0.500	0.900	10.8	0.030	0.027	2.60959E-10
4415	0.500	0.900	10.8	0.030	0.027	2.60959E-10
4365	0.500	0.900	10.8	0.030	0.027	2.60959E-10
4315	0.500	0.900	10.8	0.030	0.027	2.60959E-10
4265	0.500	0.900	10.8	0.030	0.027	2.60959E-10
4215	0.500	0.900	10.8	0.030	0.027	2.60959E-10
4165	0.500	0.900	10.8	0.030	0.027	2.60959E-10
4115	0.500	0.900	10.8	0.030	0.027	2.60959E-10
4065	0.500	0.900	10.8	0.030	0.027	2.60959E-10
4015	0.500	0.900	10.8	0.030	0.027	2.60959E-10
3965	0.500	0.900	10.8	0.030	0.027	2.60959E-10
3915	0.500	0.900	10.8	0.030	0.027	2.60959E-10
3865	0.500	0.900	10.8	0.030	0.027	2.60959E-10
3815	0.500	0.900	10.8	0.030	0.027	2.60959E-10
3765	0.500	0.900	10.8	0.030	0.027	2.60959E-10
3715	0.500	0.900	10.8	0.030	0.027	2.60959E-10
3665	0.500	0.900	10.8	0.030	0.027	2.60959E-10
3615	0.500	0.900	10.8	0.030	0.027	2.60959E-10
3565	0.500	0.900	10.8	0.030	0.027	2.60959E-10

Groundwater Recharge Distribution for 15 ka						
Altitude (ft)	Precipitation (ft)	P-15ka	Precipitation (in)	Effective recharge	Recharge (ft/yr)	Recharge (m/yr)
10715	1.800	1.440	17.28	0.150	0.216	2.08767E-09
10615	1.800	1.440	17.28	0.150	0.216	2.08767E-09
10565	1.800	1.440	17.28	0.150	0.216	2.08767E-09
10515	1.800	1.440	17.28	0.150	0.216	2.08767E-09
10465	1.800	1.440	17.28	0.150	0.216	2.08767E-09
10415	1.800	1.440	17.28	0.150	0.216	2.08767E-09
10365	1.800	1.440	17.28	0.150	0.216	2.08767E-09
10315	1.800	1.440	17.28	0.150	0.216	2.08767E-09
10265	1.800	1.440	17.28	0.150	0.216	2.08767E-09
10215	1.800	1.440	17.28	0.150	0.216	2.08767E-09
10165	1.800	1.440	17.28	0.150	0.216	2.08767E-09
10115	1.800	1.440	17.28	0.150	0.216	2.08767E-09
10065	1.800	1.440	17.28	0.150	0.216	2.08767E-09
10015	1.800	1.440	17.28	0.150	0.216	2.08767E-09
9965	1.800	1.440	17.28	0.150	0.216	2.08767E-09
9915	1.800	1.440	17.28	0.150	0.216	2.08767E-09
9865	1.800	1.440	17.28	0.150	0.216	2.08767E-09
9815	1.800	1.440	17.28	0.150	0.216	2.08767E-09
9765	1.800	1.440	17.28	0.150	0.216	2.08767E-09
9715	1.800	1.440	17.28	0.150	0.216	2.08767E-09
9665	1.800	1.440	17.28	0.150	0.216	2.08767E-09
9615	1.800	1.440	17.28	0.150	0.216	2.08767E-09
9565	1.800	1.440	17.28	0.150	0.216	2.08767E-09
9515	1.800	1.440	17.28	0.150	0.216	2.08767E-09
9465	1.800	1.440	17.28	0.150	0.216	2.08767E-09
9415	1.800	1.440	17.28	0.150	0.216	2.08767E-09
9365	1.800	1.440	17.28	0.150	0.216	2.08767E-09
9315	1.800	1.440	17.28	0.150	0.216	2.08767E-09
9265	1.800	1.440	17.28	0.150	0.216	2.08767E-09
9215	1.800	1.440	17.28	0.150	0.216	2.08767E-09
9165	1.800	1.440	17.28	0.150	0.216	2.08767E-09
9115	1.800	1.440	17.28	0.150	0.216	2.08767E-09
9065	1.800	1.440	17.28	0.150	0.216	2.08767E-09
9015	1.800	1.440	17.28	0.150	0.216	2.08767E-09
8965	1.500	1.200	14.4	0.070	0.084	8.11872E-10
8915	1.500	1.200	14.4	0.070	0.084	8.11872E-10
8865	1.500	1.200	14.4	0.070	0.084	8.11872E-10
8815	1.500	1.200	14.4	0.070	0.084	8.11872E-10

8765	1.500	1.200	14.4	0.070	0.084	8.11872E-10
8715	1.500	1.200	14.4	0.070	0.084	8.11872E-10
8665	1.500	1.200	14.4	0.070	0.084	8.11872E-10
8615	1.500	1.200	14.4	0.070	0.084	8.11872E-10
8565	1.500	1.200	14.4	0.070	0.084	8.11872E-10
8515	1.500	1.200	14.4	0.070	0.084	8.11872E-10
8465	1.500	1.200	14.4	0.070	0.084	8.11872E-10
8415	1.500	1.200	14.4	0.070	0.084	8.11872E-10
8365	1.500	1.200	14.4	0.070	0.084	8.11872E-10
8315	1.500	1.200	14.4	0.070	0.084	8.11872E-10
8265	1.500	1.200	14.4	0.070	0.084	8.11872E-10
8215	1.500	1.200	14.4	0.070	0.084	8.11872E-10
8165	1.500	1.200	14.4	0.070	0.084	8.11872E-10
8115	1.500	1.200	14.4	0.070	0.084	8.11872E-10
8065	1.500	1.200	14.4	0.070	0.084	8.11872E-10
8015	1.500	1.200	14.4	0.070	0.084	8.11872E-10
7965	1.100	0.880	10.56	0.030	0.0264	2.55160E-10
7915	1.100	0.880	10.56	0.030	0.0264	2.55160E-10
7865	1.100	0.880	10.56	0.030	0.0264	2.55160E-10
7815	1.100	0.880	10.56	0.030	0.0264	2.55160E-10
7765	1.100	0.880	10.56	0.030	0.0264	2.55160E-10
7715	1.100	0.880	10.56	0.030	0.0264	2.55160E-10
7665	1.100	0.880	10.56	0.030	0.0264	2.55160E-10
7615	1.100	0.880	10.56	0.030	0.0264	2.55160E-10
7565	1.100	0.880	10.56	0.030	0.0264	2.55160E-10
7515	1.100	0.880	10.56	0.030	0.0264	2.55160E-10
7465	1.100	0.880	10.56	0.030	0.0264	2.55160E-10
7415	1.100	0.880	10.56	0.030	0.0264	2.55160E-10
7365	1.100	0.880	10.56	0.030	0.0264	2.55160E-10
7315	1.100	0.880	10.56	0.030	0.0264	2.55160E-10
7265	1.100	0.880	10.56	0.030	0.0264	2.55160E-10
7215	1.100	0.880	10.56	0.030	0.0264	2.55160E-10
7165	1.100	0.880	10.56	0.030	0.0264	2.55160E-10
7115	1.100	0.880	10.56	0.030	0.0264	2.55160E-10
7065	1.100	0.880	10.56	0.030	0.0264	2.55160E-10
7015	1.100	0.880	10.56	0.030	0.0264	2.55160E-10
6965	0.800	0.640	7.68	0.000	0	0
6915	0.800	0.640	7.68	0.000	0	0
6865	0.800	0.640	7.68	0.000	0	0

Groundwater Recharge Distribution for 18 ka

Altitude (ft)	Precipitation (ft)	P-18ka	Precipitation (in)	Effective recharge	Recharge (ft/yr)	Recharge (m/yr)
10715	1.800	2.250	27	0.250	0.5625	5.43664E-09
10615	1.800	2.250	27	0.250	0.5625	5.43664E-09
10565	1.800	2.250	27	0.250	0.5625	5.43664E-09
10515	1.800	2.250	27	0.250	0.5625	5.43664E-09
10465	1.800	2.250	27	0.250	0.5625	5.43664E-09
10415	1.800	2.250	27	0.250	0.5625	5.43664E-09
10365	1.800	2.250	27	0.250	0.5625	5.43664E-09
10315	1.800	2.250	27	0.250	0.5625	5.43664E-09
10265	1.800	2.250	27	0.250	0.5625	5.43664E-09
10215	1.800	2.250	27	0.250	0.5625	5.43664E-09
10165	1.800	2.250	27	0.250	0.5625	5.43664E-09
10115	1.800	2.250	27	0.250	0.5625	5.43664E-09
10065	1.800	2.250	27	0.250	0.5625	5.43664E-09
10015	1.800	2.250	27	0.250	0.5625	5.43664E-09
9965	1.800	2.250	27	0.250	0.5625	5.43664E-09
9915	1.800	2.250	27	0.250	0.5625	5.43664E-09
9865	1.800	2.250	27	0.250	0.5625	5.43664E-09
9815	1.800	2.250	27	0.250	0.5625	5.43664E-09
9765	1.800	2.250	27	0.250	0.5625	5.43664E-09
9715	1.800	2.250	27	0.250	0.5625	5.43664E-09
9665	1.800	2.250	27	0.250	0.5625	5.43664E-09
9615	1.800	2.250	27	0.250	0.5625	5.43664E-09
9565	1.800	2.250	27	0.250	0.5625	5.43664E-09
9515	1.800	2.250	27	0.250	0.5625	5.43664E-09
9465	1.800	2.250	27	0.250	0.5625	5.43664E-09
9415	1.800	2.250	27	0.250	0.5625	5.43664E-09
9365	1.800	2.250	27	0.250	0.5625	5.43664E-09
9315	1.800	2.250	27	0.250	0.5625	5.43664E-09
9265	1.800	2.250	27	0.250	0.5625	5.43664E-09
9215	1.800	2.250	27	0.250	0.5625	5.43664E-09
9165	1.800	2.250	27	0.250	0.5625	5.43664E-09
9115	1.800	2.250	27	0.250	0.5625	5.43664E-09
9065	1.800	2.250	27	0.250	0.5625	5.43664E-09
9015	1.800	2.250	27	0.250	0.5625	5.43664E-09
8965	1.500	1.875	22.5	0.250	0.46875	4.53054E-09
8915	1.500	1.875	22.5	0.250	0.46875	4.53054E-09
8865	1.500	1.875	22.5	0.250	0.46875	4.53054E-09
8815	1.500	1.875	22.5	0.250	0.46875	4.53054E-09



8765	1.500	1.875	22.5	0.250	0.46875	4.53054E-09
8715	1.500	1.875	22.5	0.250	0.46875	4.53054E-09
8665	1.500	1.875	22.5	0.250	0.46875	4.53054E-09
8615	1.500	1.875	22.5	0.250	0.46875	4.53054E-09
8565	1.500	1.875	22.5	0.250	0.46875	4.53054E-09
8515	1.500	1.875	22.5	0.250	0.46875	4.53054E-09
8465	1.500	1.875	22.5	0.250	0.46875	4.53054E-09
8415	1.500	1.875	22.5	0.250	0.46875	4.53054E-09
8365	1.500	1.875	22.5	0.250	0.46875	4.53054E-09
8315	1.500	1.875	22.5	0.250	0.46875	4.53054E-09
8265	1.500	1.875	22.5	0.250	0.46875	4.53054E-09
8215	1.500	1.875	22.5	0.250	0.46875	4.53054E-09
8165	1.500	1.875	22.5	0.250	0.46875	4.53054E-09
8115	1.500	1.875	22.5	0.250	0.46875	4.53054E-09
8065	1.500	1.875	22.5	0.250	0.46875	4.53054E-09
8015	1.500	1.875	22.5	0.250	0.46875	4.53054E-09
7965	1.100	1.375	16.5	0.150	0.20625	1.99344E-09
7915	1.100	1.375	16.5	0.150	0.20625	1.99344E-09
7865	1.100	1.375	16.5	0.150	0.20625	1.99344E-09
7815	1.100	1.375	16.5	0.150	0.20625	1.99344E-09
7765	1.100	1.375	16.5	0.150	0.20625	1.99344E-09
7715	1.100	1.375	16.5	0.150	0.20625	1.99344E-09
7665	1.100	1.375	16.5	0.150	0.20625	1.99344E-09
7615	1.100	1.375	16.5	0.150	0.20625	1.99344E-09
7565	1.100	1.375	16.5	0.150	0.20625	1.99344E-09
7515	1.100	1.375	16.5	0.150	0.20625	1.99344E-09
7465	1.100	1.375	16.5	0.150	0.20625	1.99344E-09
7415	1.100	1.375	16.5	0.150	0.20625	1.99344E-09
7365	1.100	1.375	16.5	0.150	0.20625	1.99344E-09
7315	1.100	1.375	16.5	0.150	0.20625	1.99344E-09
7265	1.100	1.375	16.5	0.150	0.20625	1.99344E-09
7215	1.100	1.375	16.5	0.150	0.20625	1.99344E-09
7165	1.100	1.375	16.5	0.150	0.20625	1.99344E-09
7115	1.100	1.375	16.5	0.150	0.20625	1.99344E-09
7065	1.100	1.375	16.5	0.150	0.20625	1.99344E-09
7015	1.100	1.375	16.5	0.150	0.20625	1.99344E-09
6965	0.800	1.000	12	0.030	0.03	2.89954E-10
6915	0.800	1.000	12	0.030	0.03	2.89954E-10
6865	0.800	1.000	12	0.030	0.03	2.89954E-10
6815	0.800	1.000	12	0.030	0.03	2.89954E-10
6765	0.800	1.000	12	0.030	0.03	2.89954E-10
6715	0.800	1.000	12	0.030	0.03	2.89954E-10

6665	0.800	1.000	12	0.030	0.03	2.89954E-10
6615	0.800	1.000	12	0.030	0.03	2.89954E-10
6565	0.800	1.000	12	0.030	0.03	2.89954E-10
6515	0.800	1.000	12	0.030	0.03	2.89954E-10
6465	0.800	1.000	12	0.030	0.03	2.89954E-10
6415	0.800	1.000	12	0.030	0.03	2.89954E-10
6365	0.800	1.000	12	0.030	0.03	2.89954E-10
6315	0.800	1.000	12	0.030	0.03	2.89954E-10
6265	0.800	1.000	12	0.030	0.03	2.89954E-10
6215	0.800	1.000	12	0.030	0.03	2.89954E-10
6165	0.800	1.000	12	0.030	0.03	2.89954E-10
6115	0.800	1.000	12	0.030	0.03	2.89954E-10
6065	0.800	1.000	12	0.030	0.03	2.89954E-10
6015	0.800	1.000	12	0.030	0.03	2.89954E-10
5965	0.500	0.625	7.5	0.000	0	0
5915	0.500	0.625	7.5	0.000	0	0
5865	0.500	0.625	7.5	0.000	0	0

## REFERENCES

- Anderson, M.P., and Woessner, W.W., 1992. Applied groundwater modeling, Academic Press, San Diego, 381 p.
- Avon, L., and Durbin, T.J., 1994. Evaluation of the Maxey-Eakin method for estimating recharge to ground-water basins in Nevada, Water Resources Bulletin, American Water Resources Association, 30(1), 99-111.
- Barnes, C.J., Chambers, L.A., Herczeg, A.L., Jacobson, G., Williams, B.G., and Wooding, R.A., 1990. Mixing processes between saline groundwater and evaporation brines in groundwater discharge zones, Proceeding, International Conference on Groundwater in Large Sedimentary Basins, Australian Water Resources Council, Series 20, Canberra, Perth, 369-378.
- Bouwer, H., 1978. Groundwater hydrology: McGraw- Hill, New York, NY, 468 p.
- Carrera, J., 1993. An overview of uncertainties in modelling groundwater solute transport, Journal of Contaminant Hydrology, 13, 23-48.
- Diaw E.B., Lehmann, F., and Ackerer, Ph., 2001. One-dimensional simulation of solute transfer in saturated–unsaturated porous media using the discontinuous finite elements method, Journal of Contaminant Hydrology, 51, 197-213.
- Domenico, P.A., 1972. Concepts and models in groundwater hydrology, McGraw-Hill, New York, 405 p.

- Dong, W., 2004. Extraction of Paleohydrology and Paleoclimate Proxies for Unsaturated Zones and Paleolake Records in the Southwestern Great Basin, University of Nevada Las Vegas, Dissertation, 180 p.
- Dong, W., Yu, Z., and Weber, D., 2003. Simulations on water variation in arid regions. *Journal of Hydrology*, 275, 165-181.
- Doughty, C., 1999. Investigation of conceptual and numerical approaches for evaluating moisture, gas, chemical, and heat transport in fractured unsaturated rock, *Journal of Contaminant Hydrology*, 38, 69-106.
- Duffy, C.J., and Al-Hassen, S., 1988. Groundwater circulation in a closed desert basin: Topographic scaling and climatic forcing, *Water Resources Research*, 24, 1,675-1,688.
- Fan, Y., and Duffy, C.J., 1993. Monthly temperature and precipitation fields on a storm-facing mountain front: statistical structure and empirical parameterization, *Water Resources Research*, 29, 4, 157-4,166.
- Fan, Y., Duffy, C.J., and Oliver, D.S., 1997. Density-driven groundwater flow in closed desert basins: Field investigations and numerical experiments, *Journal of Hydrology*, 196, 139-184.
- Fenneman, N.M., 1931. *Physiography of western united states*, McGraw-Hill, New York, 534 p.
- Harrill, J.R., Welch, A.H., Prudic, D.E., Thomas, J.M., Carman, R.L., Plume, R.W., Gates, J.S., and Mason, J.L., 1983. *Aquifer systems in the great basin Region of Nevada, Utah, and Adjacent States-a Study Plan*, USGS Open-file Report 82- 445, 49 p.

- Holzbecher E., 1998. Modeling density-driven flow in Porous Media, Springer, Heidelberg, 286 p.
- Langbein, W.B., 1961. Salinity and hydrology of closed lakes, U.S. Geological Survey, Washington, D.C., 412 p.
- Lines, G. C., 1979. Hydrology and surface morphology of the Bonneville Salt Flats and Pilot Valley playa, Utah, U.S. Geological Survey Water-Supply paper, 2057, 107 p.
- Maasland, M., 1957. Soil anisotropy and land drainage. In: J.N., Luthin (Editor) Drainage of agricultural lands, Agron. Monogr. 7, American Society of Agronomy, Madison, Wisconsin,
- Mason, J.L., and Kipp, K.L., Jr., 1998. Hydrology of the Bonneville Salt Flats, northwestern Utah, and the simulation of ground-water flow and solute transport in the shallow-brine aquifer: U.S. Geological Survey Professional Paper, 1585, 108 p.
- Maxey, G.B., and Eakin, T.E., 1949. Groundwater in the White River Valley, White Pine, Nye, and Lincoln counties, Nevada, Water Resources Bulletin, 8, State of Nevada, Office of the state Engineer, Carson City, Nevada, 61 p.
- McCleary, K.L., 1989. Density dependent convective flow in closed basins, Thesis, Utah State University.
- Mifflin, M.D., and Wheat, M.M., 1979. Pluvial lakes and estimated pluvial climates of Nevada, Nevada Bureau of Mines and Geology Bulletin, 94, 57 p.
- Morrison, R.B., 1966. Predecessors of Great Salt Lake, Utah geological society, Salt Lake city, 77-104.
- Morrison, R.B., 1966. Predecessors of Great Salt Lake: Utah Geological Society. Guidebook to the Geology of Utah, 20, 77-104.

- Morrison, R.B., 1968. Pluvial lakes. In: J.T., Neal (Editor), Playas and dried lakes: Occurrence and development. Benchmark Papers in Geology, 20, 14-24.
- Morrison, R.B., 1991. Quaternary stratigraphic, hydrologic and climatic history of the Great Basin, with emphasis on lakes Lahontan, Bonneville and Tecopa, in the geology of North America, K-2: Quaternary non-glacial geology: Conterminous U.S., Geological Society of America, 283-320.
- Neal, J.T., 1965. Geology, mineralogy, and hydrology of U.S. playas, Air force Cambridge Research Laboratories, Bedford, Massachusetts.
- Pruess, K., Faybishenko, B., and Bodvarsson, G.S., 1999. Alternative concepts and approaches for modeling flow and transport in thick unsaturated zones of fractured rocks, Journal of Contaminant Hydrology - Special Issue, 38, 281-322.
- Ranjan, S.P., Kazama, S., and Sawamoto, M., 2005. Effects of climate and land use changes on groundwater resources in coastal aquifers, Journal of Environmental Management, 1-11.
- Simmons, C.T., Fenstemaker, T.R., and Sharp, J.M., Jr., 2001. Variable-density groundwater flow and solute transport in heterogeneous porous media: Approaches, Resolutions and Future Challenges, Journal of Contaminant Hydrology, 52, 245-275.
- Simmers, I., 1987. Estimation of natural groundwater recharge, D. Reidel Publishing Co., Boston, 510.
- Simmers, I., 1997. Recharge of phreatic aquifers in (semi-) arid areas, A.A. Balkema, Netherlands, 277.
- Smith, G.I., and Bischoff, J.L., 1997. Core OL-92 from Owens Lake: Project rationale, geologic setting, drilling procedures, and summary. In "An 800,000-year

- paleoclimatic record from core OL-92, Owens Lake, Southern California" edited by Smith, G.I. and Bischoff, J.L. Special Paper 317, the Geological Society of America, Boulder, 165.
- Smith, A. J., and Jeffrey, V.T., 2001. Density-dependent surface water-groundwater interaction and nutrient discharge in the Swan- Canning Estuary, Center for groundwater studies, Australia, *Hydrological Processes*, 15, 2,595-2,616.
- Snyder, C.T., 1962. A hydrologic classification of valleys in the Great Basin, *International Association of Scientific Hydrology Bulletin*, 7, 53 - 59.
- Snyder, C.T., and Langbein, W.T., 1962. The Pleistocene Lake in Spring Valley Nevada and its climatic implications, *Journal Geophysics Research*, 67, 2,385-2,394.
- Souza, W.R., 1987. Documentation of a graphical display program for the Saturated-Unsaturated Transport (SUTRA) finite-element simulation model, U.S. Geological Survey Water Resources Investigations Report, 87-4245, 122 p.
- Thompson, R.S., Whitlock, C., Bartlein, P.J., Harrison, S.P., and Spaulding, W.G., 1994. Climatic changes in the western United States since 18,000 yr B.P., in Wright et al, eds., *Global Climates since the Last Glacial Maximum*. University of Minnesota Press, 468-513.
- Thompson, R.S., Anderson, K.H., and Bartlein, P.J., 1999. Quantitative paleoclimatic reconstructions from late Pleistocene plant macrofossils of the yucca mountain region. U.S. Geological Survey Open-File Report 99-338.
- Voss, C.I., 1984. A finite-element simulation model for saturated-unsaturated, fluid-density-dependent ground-water flow with energy transport or chemically reactive

- single-species solute transport: U.S. Geological Survey Water-Resources Investigation Report, 84-4369, 409 p.
- Voss, C.I., and Provost, A.M., 2002. SUTRA, a model for saturated-unsaturated variable-density ground-water flow with solute or energy transport, Water-Resources Investigations Report, 02-4231, Reston, Virginia: USGS, 260 p.
- Weissmann, G.S., and Fogg, G.E., 1999. Multi-scale alluvial fan heterogeneity modeled with transition probability geostatistics in a sequence stratigraphic framework: Journal of Hydrology, 226, 48-65.
- Wooding, R.A., 1978. Large-scale geothermal field parameters and convection theory, New Zealand Journal of Science, 27, 219-228.
- Wooding, R.A., Tyler, S.W., and White, I., 1997. Convection in groundwater below an evaporating salt lake: 1. Onset of instability, Water Resources Research, 33, 1,199-1,217.
- Wooding, R.A., Tyler, S.W., White, I., and Anderson, P.A., 1997. Convection in groundwater below an evaporating salt lake: 2. Evolution of fingers or plumes. Water Resources Research, 33, 1,219-1,228.



## VITA

Graduate College  
University of Nevada, Las Vegas

Aron Habte

### Home Address:

1429 Canyon Rose Way  
Las Vegas, NV 89108

### Degrees:

Bachelor of Science, Soil and Water Conservation, 1996  
University of Asmara, Eritrea

### Publications:

Richard J. L., Glenn L. L., and Aron M. H., 2005, Selected ground-water data for Yucca mountain region, Southern Nevada and Eastern California, January- December 2003, USGS Open-file Report, 2005- 1286, 74 p.

Thesis Title: On Evaluating Density Driven Groundwater Flow in the Closed Basin

### Thesis Examination Committee:

Chair, Dr. Zhongbo Yu, Ph.D.  
Committee Member, Dr. David Kremer, Ph.D.  
Committee Member, Dr. Thomas C. Piechota, Ph.D.  
Graduate Faculty Representative, Dr. Ashok K, Ph.D.